

# CIAMTIS

U.S. DOT Region 3 University Transportation Center

## Design of Anchors for Rapid and Durable Strengthening of Bridges with Externally Bonded Carbon Fiber Reinforced Polymers

November 23, 2021

*Prepared by:*  
C. Viniarski, J. Tatar, and M. Head  
University of Delaware

[r3utc.psu.edu](http://r3utc.psu.edu)



**PennState**  
College of Engineering

LARSON  
TRANSPORTATION  
INSTITUTE

*DISCLAIMER*

The contents of this report reflect the views of the authors, who are responsible for the facts and the accuracy of the information presented herein. This document is disseminated in the interest of information exchange. The report is funded, partially or entirely, by a grant from the U.S. Department of Transportation's University Transportation Centers Program. However, the U.S. Government assumes no liability for the contents or use thereof.

**Technical Report Documentation Page**

<b>1. Report No.</b> CIAM-COR-R05	<b>2. Government Accession No.</b>	<b>3. Recipient's Catalog No.</b>	
<b>4. Title and Subtitle</b> Design of Anchors for Rapid and Durable Strengthening of Bridges with Externally Bonded Carbon Fiber Reinforced Polymers		<b>5. Report Date</b> November 23, 2021	
<b>7. Author(s)</b> Christian Viniarski, Jovan Tatar, Ph.D., <a href="https://orcid.org/0000-0003-4901-4019">https://orcid.org/0000-0003-4901-4019</a> Monique Head, Ph.D., P.E., <a href="https://orcid.org/0000-0002-0608-9961">https://orcid.org/0000-0002-0608-9961</a>		<b>6. Performing Organization Code</b>  <b>8. Performing Organization Report No.</b>	
<b>9. Performing Organization Name and Address</b> Department of Civil and Environmental Engineering University of Delaware DuPont Hall, 127 The Green Newark, DE 19716		<b>10. Work Unit No. (TRAVIS)</b>	
<b>12. Sponsoring Agency Name and Address</b> U.S. Department of Transportation Research and Innovative Technology Administration 3rd Fl, East Bldg E33-461 1200 New Jersey Ave, SE Washington, DC 20590		<b>11. Contract or Grant No.</b> 69A3551847103	
<b>15. Supplementary Notes</b> Work funded through The Pennsylvania State University through the University Transportation Center Grant Agreement, Grant No. 69A3551847103.		<b>13. Type of Report and Period Covered</b> Final Report 03/01/2019 – 08/31/2021	
<b>16. Abstract</b> This study investigates the effectiveness of U-Wraps as a method of flexural anchorage. A total of 12 structural-scale reinforced concrete girders were tested in flexure to examine the effect U-Wraps have on strength gain and ductility. Out of the 12 reinforced concrete girders, 8 girders were strengthened flexurally with CFRP and then anchored with U-Wraps. The remaining 4 girders were used as control specimens. The primary variable that was investigated was the area of U-Wraps compared to the area of longitudinal CFRP installed on a girder. The ratio of the area of the U-Wraps to the area of the longitudinal CFRP was compared to the existing literature data to investigate the effect U-Wraps have on strength gain and ductility. The ultimate goal is to use the findings from the comparison of the experimental data and literature data to influence future design provisions. The future design provisions will account for the increase in load capacity, increase in ductility, and a shift of the failure modes due to the addition of U-Wraps as flexural anchors to flexural CFRP.		<b>14. Sponsoring Agency Code</b>	
<b>17. Key Words</b> Reinforced concrete girder, carbon fiber reinforced polymer, flexural anchorage, ductility, U-Wrap		<b>18. Distribution Statement</b> No restrictions. This document is available from the National Technical Information Service, Springfield, VA 22161	
<b>19. Security Classif. (of this report)</b> Unclassified	<b>20. Security Classif. (of this page)</b> Unclassified	<b>21. No. of Pages</b> 94	<b>22. Price</b>

## Table of Contents

LIST OF TABLES .....	IV
LIST OF FIGURES .....	V
INTRODUCTION .....	1
BACKGROUND INFORMATION .....	1
OBJECTIVE AND SCOPE .....	3
LITERATURE REVIEW .....	4
INTRODUCTION .....	4
U-WRAPs.....	5
FIBER ANCHORS .....	8
KNOWLEDGE GAPS .....	12
DESIGN AND CONSTRUCTION OF SPECIMENS .....	15
DESIGN OF REINFORCED CONCRETE GIRDERS .....	15
DESIGN OF STRENGTHENED REINFORCED CONCRETE GIRDERS .....	16
Test Matrix.....	16
CFRP INSTALLATION.....	21
Surface Preparation.....	21
CFRP Installation.....	22
EXPERIMENTAL TEST SETUP .....	27
TEST SETUP .....	27
THREE-DIMENSIONAL DIGITAL IMAGE CORRELATION SYSTEM .....	28
GIRDER INSTRUMENTATION.....	29
CHARACTERIZATION OF MATERIALS PROPERTIES .....	31
CONCRETE MATERIAL PROPERTIES.....	31
REINFORCING STEEL MATERIAL PROPERTIES .....	36
CARBON FIBER REINFORCED POLYMERS MATERIAL PROPERTIES .....	38
RESULTS AND DISCUSSION .....	42
FLEXURAL BEHAVIOR .....	42
STRAIN IN LONGITUDINAL CFRP .....	50
COMPARISON TO MODELS .....	54
COMPARISON TO LITERATURE.....	56
SUMMARY AND CONCLUSIONS .....	64
SUMMARY .....	64
CONCLUSIONS.....	65
RECOMMENDATIONS FOR FUTURE WORK .....	64
REFERENCES .....	65
APPENDIX.....	68

## List of Tables

Table 1.	Anchorage ratios for each of the 12 girders.....	19
Table 2.	Concrete mix design .....	31
Table 3.	Concrete material properties .....	32
Table 4.	Results from compressive cylinder testing at 665 days.....	35
Table 5.	Results from fracture energy tests of concrete at 684 days .....	36
Table 6.	Results of #6 rebar tensile tests.....	38
Table 7.	CFRP tensile coupon test results.....	41
Table 8.	Summary of Test Results .....	43
Table 9.	Descriptive process on the creation of witness panels.....	68
Table 10.	Experimental data and literature data used in Figure 65.....	81
Table 11.	Experimental data and literature data used in Figure 67.....	82

## List of Figures

Figure 1.	Shear strengthening of bridge girders using CFRP U-Wraps (The Constructor, 2020) .....	1
Figure 2.	CFRP strengthening of bridge piers (Florida International University, 2019) .....	2
Figure 3.	Flexural strengthening of bridge girders using CFRP (Concrete Protection & Repair Services, 2019) .....	2
Figure 4.	Different types of anchorage systems for flexural CFRP (ACI Committee 440, 2017) .....	3
Figure 5.	Typical debonding failure modes (ACI Committee 440, 2017) .....	5
Figure 6.	U-Wraps provided along the entire shear span (Hasnat et al., 2016) .....	6
Figure 7.	90-degree (left) and Inclined U-Wrap (right) (ACI Committee 440, 2017) .....	7
Figure 8.	U-Wraps anchored with fiber anchors (CMAS anchors) (Demakos et al., 2013) .....	8
Figure 9.	Fiber anchor variables .....	9
Figure 10.	Dry single-fan (left) and bow-tie (right) fiber anchors (Smith et al., 2013) .....	9
Figure 11.	Test iterations from Zaki & Rasheed (2019) .....	10
Figure 12.	Test iteration from Smith et al. (2013) .....	11
Figure 13.	Angle of insertion (Smith et al., 2013) .....	11
Figure 14.	½” fillet at the edge of the anchor hole (Jirsa et al., 2017) .....	12
Figure 15.	Reinforcement layout of the girder .....	15
Figure 16.	Cross-section of the reinforcement layout of the girder .....	16
Figure 17.	Example of the nomenclature used for the girders .....	16
Figure 18.	Control girders used in the study .....	17
Figure 19.	Test matrix of flexurally strengthened girders with U-Wrap anchorage .....	20
Figure 20.	Numeric labels used to denote U-Wraps spaced at 8 in. on-center. U-Wraps 1, 3, 5, 7, 10, 12, 14, and 16 were used on the girder with U-Wraps spaced at 16 in. on-center (1L2U-16). .....	20
Figure 21.	Confirming the CSP of the concrete using an ICRI surface profile coupon .....	21
Figure 22.	Typical ground edge of a girder .....	22
Figure 23.	Cleaning the surface of the concrete with compressed air .....	22
Figure 24.	Measuring the weight of the Part A component of the epoxy .....	23
Figure 25.	Mixing the epoxy in a 5-gallon bucket using a paddle drill mixer .....	23
Figure 26.	Applying epoxy to the concrete substrate using an epoxy roller .....	23
Figure 27.	Applying thickened epoxy to the tensile face of the girder using a plastic putty knife. ....	24
Figure 28.	Thickened epoxy applied to the vertical face of the girder at the locations of the U-Wraps .....	24
Figure 29.	Spreading epoxy on the dry-fibers using a putty knife within the epoxy bath .....	25

Figure 30.	Rolling the saturated fiber onto a section of PVC .....	25
Figure 31.	Installing the longitudinal sheet of CFRP onto the tensile face of the girder .....	25
Figure 32.	Smoothing the CFRP onto the surface of the beam using putty knife.....	26
Figure 33.	Installing U-Wraps onto the girder .....	26
Figure 34.	3D Diagrams of the test setup: (a) Elevation view of the test setup; (b) Isometric view of the test setup.....	27
Figure 35.	Photographs of the test setup: (a) Elevation view of the test setup; (b) Wide shot of the test setup.....	28
Figure 36.	Photographs of the DIC system test (red arrows showing DIC cameras): (a) DIC System placed on top of the aluminum column; (b) Test setup with the DIC system (red arrows showing DIC cameras) .....	28
Figure 37.	Calibration cross used for the DIC system .....	29
Figure 38.	Speckled pattern applied to the vertical and tension faces of the girder.....	29
Figure 39.	LVDT loaded against the aluminum plate adhered to the girder.....	30
Figure 40.	Typical instrumentation plan of a girder.....	30
Figure 41.	Filling concrete into 4 in. x 8 in. cylinder molds.....	32
Figure 42.	Finishing concrete within a 6 in. x 6 in. x 20 in. beam mold.....	32
Figure 43.	Grinding the top surface of the concrete cylinder.....	34
Figure 44.	Typical end result of grinding the top surface of a concrete cylinder .....	34
Figure 45.	Load versus displacement curves from fracture energy tests .....	35
Figure 46.	Typical 4-foot section of #6 rebar used for tensile tests .....	36
Figure 47.	Ruptured rebar tensile test specimen .....	37
Figure 48.	Stress strain curves of #6 rebar tensile test specimens .....	38
Figure 49.	Drawing of CFRP tensile coupons.....	39
Figure 50.	Typical failure mode observed during CFRP tensile testing .....	40
Figure 51.	Results from the CFRP tensile coupon tests .....	40
Figure 52.	Load versus midspan deflection plots of all 12 girders tested.....	43

Figure 53.	Typical failure modes in CFRP-strengthened beams: (a) Concrete crushing (3L3U-8) (arrow points to the primary failure mode of concrete crushing); (b) IC debonding (2L0U); (c) longitudinal CFRP rupture (1L1U-8); (d) U-Wrap anchor rupture (arrows point to ruptured anchors on girder 2L1U-8); (e) complete debonding of U-Wrap anchor (arrow points to debonded anchors on girder 2L2U-8); (f) partial debonding of U-Wrap anchor (arrow points to partially debonded anchor on girder 2L3U-8); (g) U-Wrap interface failure in Girder 2L2U-8 (dashed lines outline the U-Wrap anchor) .....	45
Figure 54.	Sounding the U-Wraps to determine whether the U-Wraps are partially debonded.....	46
Figure 55.	Post-mortem inspection of girders with U-Wrap anchorage (● complete U-Wrap debonding, ○ partial U-Wrap debonding, ▲ U-Wrap Rupture, — longitudinal CFRP rupture or concrete crushing, ■ U-Wrap interface failure).....	48
Figure 56.	Summary of ductility coefficients of all 12 girders .....	49
Figure 57.	Typical crack patterns at failure (arrows represent the approximate locations of the loading points on the girder and shaded bars represent the approximate locations of the U-Wraps): (a) Girder 1L1U-8; (b) Girder 1L2U-16 .....	50
Figure 58.	Summary of maximum strains of the longitudinal CFRP.....	51
Figure 59.	Comparison of strains along the length of the unanchored control girders at flexural capacity (Vertical dashed lines show the limits of the constant moment region).....	52
Figure 60.	Example peak U-Wrap strain data from girder 2L2U-8 .....	53
Figure 61.	Summary of peak U-Wrap strains observed in the anchored girders (Range bars indicate the maximum and minimum observed strains in the U-Wraps).....	53
Figure 62.	Comparison of the experimental data to the Response-2000 model (◆ IC debonding, — longitudinal CFRP rupture, ● complete U-Wrap debonding, ○ partial U-Wrap debonding and U-Wrap interface failure, ▲ U-Wrap Rupture, ★ concrete crushing) .....	56
Figure 63.	Comparison of strain of the steel and concrete from the Response-2000 model to the ACI 318 tension-controlled limits. ....	56
Figure 64.	Load versus midspan deflection plot used to illustrate calculation of the CFRP contribution .....	57
Figure 65.	Normalized CFRP contribution versus the anchorage ratio of the literature data and experimental data from this study (Experimental data from this study is indicated with red ellipses) .....	58
Figure 66.	Graphical representation of effect of unstrengthened control beam strain hardening behavior on the apparent CFRP contribution to the overall load capacity .....	59



Figure 67.	Experimental moment capacity versus the predicted moment capacity using $\kappa_U$ account for the addition of U-Wraps to the longitudinal CFRP: (a) All 38 specimens between literature data and experimental data; (b) Specimens with an anchorage ratio greater than 1.50 and evenly distributed U-Wrap anchors .....	61
Figure 68.	Predicted versus experimental values of the CFRP contribution to the moment capacity: (a) All 28 specimens from the literature and experimental data reviewed; (b) 9 of the 28 specimens that had an anchorage ratio of at least 1.50, had evenly distributed U-Wraps, and met the surface preparation guidelines presented by ACI Committee 440 (2017) .....	63
Figure 69.	Concrete crushing failure of 0L0U .....	71
Figure 70.	IC debonding failure of 1L0U.....	71
Figure 71.	Rupture of the longitudinal CFRP within the constant moment region of 1L1U-8.....	72
Figure 72.	Rupture of the longitudinal CFRP within the constant moment region of 1L2U-16.....	72
Figure 73.	IC debonding failure of 2L0U. Girder was taken to concrete crushing post-debonding failure to investigate its residual strength. ....	73
Figure 74.	U-Wrap rupture failure of 2L1U-8 .....	73
Figure 75.	Complete U-Wrap debonding failure of 2L2U-8.....	74
Figure 76.	Partial U-Wrap debonding failure of 2L3U-8.....	74
Figure 77.	IC debonding failure of 3L0U.....	75
Figure 78.	U-Wrap rupture failure of 3L1U-8 .....	75
Figure 79.	Complete U-Wrap debonding failure of 3L2U-8.....	76
Figure 80.	Concrete crushing failure of 3L3U-8. Secondary failure mode of complete U-Wrap debonding was observed.....	76
Figure 81.	Crack patterns of the control girders (arrows represent the approximate locations of the loading points on the girder): (a) Girder 0L0U; (b) Girder 1L0U; (c) Girder 2L0U; (d) Girder 3L0U .....	77
Figure 82.	Crack patterns of the girders strengthened with 1 ply of longitudinal CFRP (arrows represent the approximate locations of the loading points on the girder and the shaded bars represent the approximate locations of the U-Wraps): (a) Girder 1L1U-8; (b) Girder 1L2U-16 .....	78
Figure 83.	Crack patterns of the girders strengthened with 2 plies of longitudinal CFRP (arrows represent the approximate locations of the loading points on the girder and the shaded bars represent the approximate locations of the U-Wraps): (a) Girder 2L1U-8; (b) Girder 2L2U-8; (c) Girder 2L3U-8 .....	79
Figure 84.	Crack patterns of the girders strengthened with 3 plies of longitudinal CFRP (arrows represent the approximate locations of the loading points on the girder and the shaded bars represent the approximate locations of the U-Wraps): (a) Girder 3L1U-8; (b) Girder 3L2U-8; (c) Girder 3L3U-8 .....	80

# CHAPTER 1

## Introduction

### BACKGROUND INFORMATION

Carbon fiber reinforced polymer (CFRP) composites have become an increasingly popular material used to externally strengthen concrete members in buildings, bridges, and parking garages. This is due to the ability of CFRP to increase the ultimate strength capacity, ductility, and stiffness when it is applied to structural concrete members. Furthermore, CFRP composites have a relatively easy installation process, allowing them to be used in projects where rapid repair and structural strengthening are required. CFRP offers many benefits compared to existing strengthening methods, such as having a high tensile strength-to-weight ratio and requiring minimal maintenance over their service life. CFRP composites are also a non-corrosive material, which can be used to strengthen structures that are prone to corrosion-related deterioration (i.e., bridges and parking garages).

Over recent years, there has been an increase in the demand to strengthen bridges. This increase comes from commonly encountered structural issues such as increased load demands, eliminating structural deficiencies due to poor construction or insufficient design, or the need to restore the load-carrying capacity in members subjected to deterioration (Wang, 2000). Due to its material properties, CFRP is currently utilized in bridge repair projects to provide additional shear resistance in girders (Figure 1), strengthen piers (column jacketing) (Figure 2), and flexurally strengthen concrete girders (Figure 4).



*Figure 1. Shear strengthening of bridge girders using CFRP U-Wraps (The Constructor, 2020).*



**Figure 2. CFRP strengthening of bridge piers (Florida International University, 2019).**

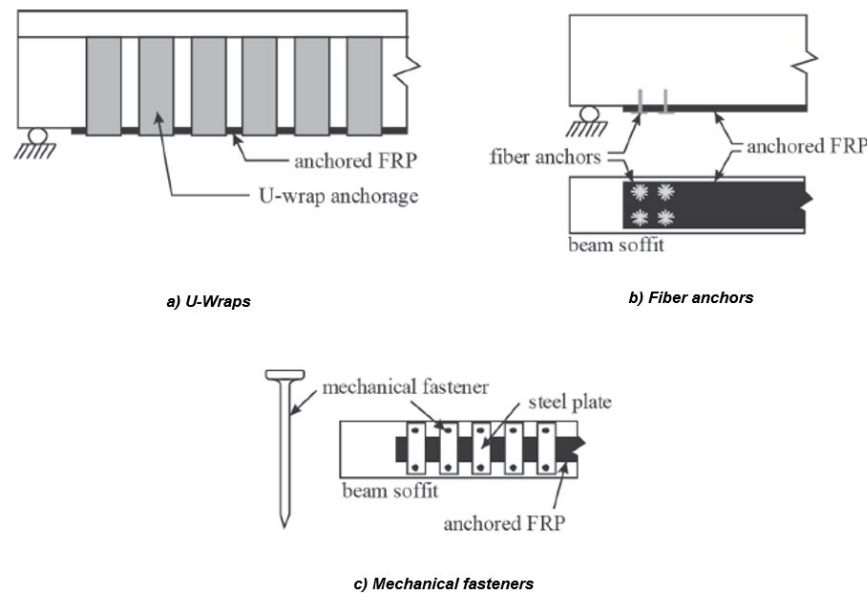


**Figure 3. Flexural strengthening of bridge girders using CFRP (Concrete Protection & Repair Services, 2019).**

(Lee & Lopez, 2016).

Different types of anchorage systems that have been investigated to delay IC debonding are fiber anchors, mechanical fasteners, and transverse strips of CFRP (herein referred to as U-Wraps) (Wang, 2000) (Figure 4). Fiber anchors and mechanical fasteners require drilling into the concrete beam, which complicates the relatively easy installation process of CFRP. Mechanical fasteners are susceptible to galvanic corrosion when coming into contact with carbon and additional corrosion-related deterioration in bridges as a result

of exposure to de-icing salts. A major benefit of using CFRP to strengthen structural members is that CFRP is a non-corrosive material. While mechanical fasteners may improve the performance of a strengthened member, they counteract the key benefit of CFRP being a non-corrosive material. A majority of the research efforts regarding delaying IC debonding have used U-Wraps as their anchorage method. U-Wraps are a popular option for anchorage, since they are made from the same material and have the same installation procedures as the flexural carbon fiber reinforced polymer sheets. U-Wraps are currently used in shear strengthening of reinforced concrete beams; however, this study focuses on their contribution toward delaying flexural debonding failure modes. When it comes to the flexural strengthening of reinforced concrete slabs, U-Wraps cannot be used due to the fact there is no vertical face to turn-up the transverse sheet. Therefore, fiber anchors are an alternative because they are also made from the same material as the laminate—a non-corrosive material. There is a non-conclusive knowledge on how these types of anchorage affect the behavior of concrete members that are flexurally strengthened with CFRP.



**Figure 4. Different types of anchorage systems for flexural CFRP (ACI Committee 440, 2017).**

## OBJECTIVE AND SCOPE

This study investigates the effectiveness of U-Wraps as a method of flexural anchorage. A total of 12 structural-scale reinforced concrete girders were tested in flexure to examine the effect U-Wraps have on strength gain and ductility. Out of the 12 reinforced concrete girders, 8 girders were strengthened flexurally with CFRP and then anchored with U-Wraps. The remaining 4 girders were used as control specimens. The primary variable that was investigated was the area of U-Wraps compared to the area of longitudinal CFRP installed on a girder. The ratio of the area of the U-Wraps to the area of the longitudinal CFRP was compared to the existing literature data to investigate the effect U-Wraps have on strength gain and ductility. The ultimate goal is to use the findings from the comparison of the experimental data and literature data to influence future design provisions. The future design provisions will account for the increase in load capacity, increase in ductility, and a shift of the failure modes due to the addition of U-Wraps as flexural anchors to flexural CFRP.

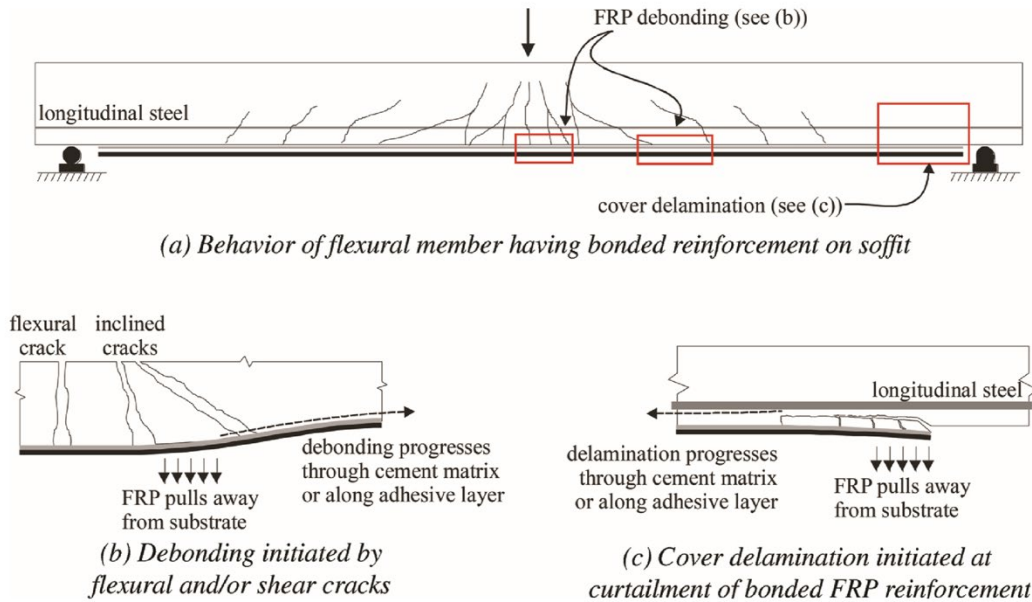
## CHAPTER 2

# Literature Review

### INTRODUCTION

As previously stated, the two governing failure modes of CFRP in flexural strengthening of concrete members are IC debonding and cover delamination. IC debonding arises when the flexural cracks start to propagate in the high moment region of the beam (Figure 5a). As a result of the flexural cracks, debonding of the laminate occurs at the location where the flexural cracks meet the laminate (Smith et al., 2011). The debonding then propagates outward from the high moment region toward the end of the beam, eventually resulting in the complete debonding of the flexural CFRP (Figure 5b). Although studies have shown that anchorage can delay or prevent IC debonding, ACI Committee 440 (2017) currently does not have any anchor design guidelines to suppress IC debonding as a failure mode (Smith et al., 2011). In an effort to maximize the utilization of the flexural CFRP and increase the load capacity of the strengthened member, researchers have investigated the effect U-Wraps and fiber anchors have on delaying IC debonding.

Cover delamination occurs when high normal stresses develop at the ends of the flexural CFRP due to the flexural CFRP trying to remain in its “level state” during the beam’s deflection. The steel reinforcement creates a weak horizontal plane, and the normal stresses in the laminate cause the concrete cover to delaminate from the soffit of the beam (Figure 5c). ACI Committee 440 (2017) currently has two separate design recommendations to suppress end peeling. ACI Committee 440 (2017) defines points to terminate the flexural CFRP based on the development of the bond between the concrete substrate and the CFRP. Additionally, ACI Committee 440 (2017) provides a design recommendation for U-Wraps to be placed as close as possible to the location of zero moment along the flexural CFRP to suppress cover delamination. Fu, Teng, et al. (2017) confirmed that the presence of U-Wraps placed at the ends of the flexural CFRP can suppress cover delamination and shift the governing failure mode toward IC debonding.



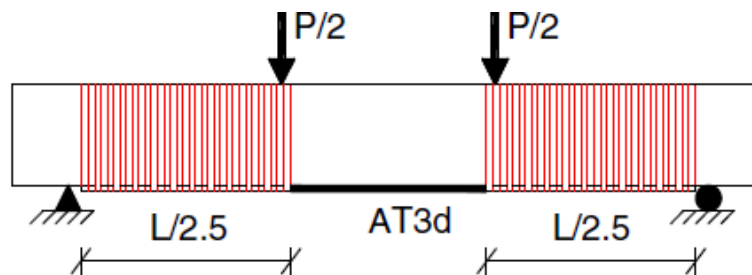
**Figure 5. Typical debonding failure modes (ACI Committee 440, 2017).**

## U-WRAPPS

U-Wraps are currently used in the shear strengthening of concrete beams or girders. However, this study focuses on their effect on delaying IC debonding and improving the performance of flexurally strengthened concrete members. U-Wraps are continuous transverse sheets of CFRP that are placed over the laminate (Figure 4a). Ideally, U-Wraps should be installed on all four sides of the beam, creating a loop. However, slabs are usually integrated into the flexural members in typical concrete construction. Therefore, U-Wraps are more commonly provided on three (3) sides of the flexural member (soffit and each vertical face). U-Wraps can increase the bond strength between the laminate and the concrete up to 125% as compared to an unanchored specimen (Haddad & Marji, 2019). The increase in bond strength provides additional resistance against the interfacial normal stresses and tensile forces developed during the loading of the member. Multiple studies were conducted investigating the effect U-Wraps have on delaying IC debonding. It has been shown that introducing U-Wraps to flexural CFRP can shift the failure mode from debonding of the laminate to rupture of the flexural CFRP, which yields the full utilization of the laminate as it reaches its rupture strain (Breña et al., 2003).

A study conducted by Hasnat et al. (2016) investigated the effect the number of plies in the U-Wraps had on the load capacity of the beam. The number of plies in the U-Wraps were changed from 1 to 2 plies throughout the different anchorage configurations used in this small-scale study. On average, adding a second ply to the U-Wraps increased the maximum load by approximately 16% (Hasnat et al., 2016). Small-scale direct shear pull-off tests concluded that increasing the number of plies in the U-Wrap from 1 to 2 yields an increase in ultimate tensile load of approximately 14% (Lee & Lopez, 2016). It should be noted that the maximum number of plies used in the U-Wraps for both studies was two and the thickness of the laminate remained constant at one ply.

Similar to increasing the number of plies in the U-Wraps, it was determined that increasing the height and width of U-Wraps can lead to additional load capacity and a more efficient utilization of the flexural CFRP (Lee & Lopez, 2016; Fu et al., 2018). Fu et al. (2018) explored the effect four different U-Wrap widths had on the flexural behavior of concrete beams strengthened with CFRP. The widths of the U-Wraps were 100 mm, 150 mm, 200 mm, and 400 mm. Each iteration resulted in an increase in maximum load as much as 14% compared to the latter. However, no further strain utilization of the flexural CFRP was shown when the width of the U-Wraps increased from 200 mm to 400 mm (Fu et al., 2018). Studies showed that providing a continuous U-Wrap for the full length of the beam (fully wrapping the beam) does not provide additional strength gain. Alternatively, it was found that fully wrapping the beam had a greater effect on reducing the ductility rather than increasing the flexural strength of a beam (Foerster, 2019). It was determined that U-Wraps placed in the high moment region of the beam contribute little to strength gain (Hasnat et al., 2016). In two separate studies, the highest load capacity was achieved when the U-wraps were provided in two plies, covered the entire shear span of the beam, and terminated at the start of the high moment region (Figure 6). Providing two-ply U-wraps at this width resulted in an increase in the maximum load of 80% and 97% compared to the unanchored test specimen (Haddad & Marji, 2019; Hasnat et al., 2016).



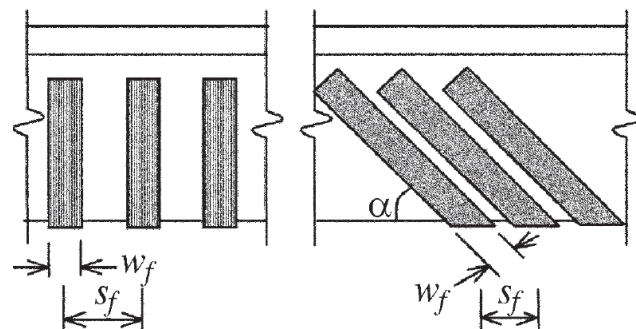
**Figure 6. U-Wraps provided along the entire shear span (Hasnat et al., 2016).**

Studies conducted by Fu et al. (2018) and Haddad & Marji (2019) both evaluated the effect the height of U-Wraps had on the load capacity and ductility of the beam. Doubling the height of the U-Wraps increased the ultimate load of a structural-scale beam by 11% (Haddad & Marji, 2019). However, increasing the height of the U-Wraps has also resulted in a decrease of ductility as much as 12% (Haddad & Marji, 2019; Fu et al., 2018). It should be noted that when the height of the U-Wraps does not exceed approximately half the height of the beam, the U-Wraps typically fail by debonding from the vertical faces of the beams (Foerster, 2019; Haddad & Marji, 2019).

A study conducted by Rasheed et al. (2015) investigated evenly distributing their U-wraps along the length of structural-scale beams. The U-wraps for each of the beams were spaced at 305 mm on-center along the entire length of the beams. The use of evenly distributed anchorage led to the full utilization of the flexural CFRP, as the beams anchored with U-wraps failed by rupture. An increase in maximum load as much as 24% was observed when evenly distributed U-Wraps were applied to the beam (Rasheed et al., 2015).

Most of the studies regarding U-Wraps as flexural anchors have consisted of vertical U-Wraps, where the fibers are oriented perpendicular to the span of the beam (herein *90-degree U-Wraps*). However, a limited number of studies have been conducted where the fibers are installed at an angle, typically at 45 degrees. Figure 7 shows a 90-degree U-Wrap and an inclined U-Wrap at angle  $\alpha$ . These studies have shown that inclined U-Wraps placed at the ends of the laminate can suppress IC debonding and further enhance the load capacity and strain utilization of the longitudinal CFRP. Increases in maximum load have been

observed as much as 52% and 60%, as compared to 90-degree U-Wraps of a similar width (Sagawa et al., 2001; Fu et al., 2018). Furthermore, inclined U-Wraps increase the strain utilization of the flexural CFRP, leading to failure modes such as rupture of the flexural CFRP, debonding of the U-Wraps, or rupture of the U-Wraps (Fu et al., 2018). It was suggested that the increases in performance can be attributed to a more efficient transfer of loads from the flexural CFRP to the U-Wraps due to the orientation of the fibers (Fu, Teng, et al., 2017; Kalfat et al., 2018). Although a limited amount of data has shown improved performance of inclined U-Wraps as compared to 90-degree U-Wraps, the orientation of the FRP sheets creates difficulties during installation. To install U-Wraps at a 45-degree angle, two separate sheets of FRP have to be used to ensure the entire surface area of the FRP sheet is in contact with the beam without any wrinkles or ridges. This results in the two separate sheets overlapping at an angle on the soffit of the beam.



**Figure 7. 90-degree (left) and Inclined U-Wrap (right) (ACI Committee 440, 2017).**

The addition of U-Wraps can mitigate IC debonding in a flexurally strengthened member. In the instances where IC debonding is suppressed, other failure modes arise. The failure mode that indicates a full utilization of the CFRP is rupture of the laminate, and in rare cases failure of concrete in compression. The rupture of the laminate results in the optimal utilization of the material as the CFRP reaches its maximum strain. Other possible failure modes that have been observed prior to rupture of the laminate are rupture of the U-Wraps and debonding of the U-Wraps. U-Wraps typically rupture at the corners of the beam due to the stress concentrations caused by the 90-degree bend in the sheet (Lee & Lopez, 2016). Thus, it was recommended to chamfer the corners of the beam to a radius of at least ½ in. to provide a smooth transition at the 90-degree bend, which lessens the stress concentrations in the U-Wraps (Lee & Lopez, 2016).

Similar to the debonding of the flexural CFRP, U-Wraps can debond from the concrete substrate. Two studies were conducted utilizing glass fiber reinforced polymer (GFRP) U-Wraps anchored with GFRP fiber anchors in conjunction with flexural carbon fiber reinforced polymer reinforcement (Figure 8) (Demakos et al., 2013; Wang, 2000). In one of the studies, introducing anchors to the U-Wraps suppressed debonding of the U-Wraps and ultimately led to the rupture of the laminate (Wang, 2000). The test specimen in the other study failed by the rupture of the fiber anchor followed by the debonding of the U-Wrap. However, the U-Wrap with fiber anchors resulted in an increase in the ultimate load-carrying capacity of approximately 17% as compared to the strengthened control beam without U-Wraps (Demakos et al., 2013). Al-Amery & Al-Mahaidi (2006) provided U-Wraps on all four sides of their flexurally strengthened small-scale beams (approximately 9-ft-long beams). Each iteration resulted in mitigating the debonding of U-Wraps and the rupture of the laminate (Al-Amery & Al-Mahaidi, 2006). While providing the U-Wrap in a continuous loop may result in the optimal failure mode of the flexural CFRP, it is rarely feasible in practical strengthening scenarios, as slabs are typically integrated into beams.



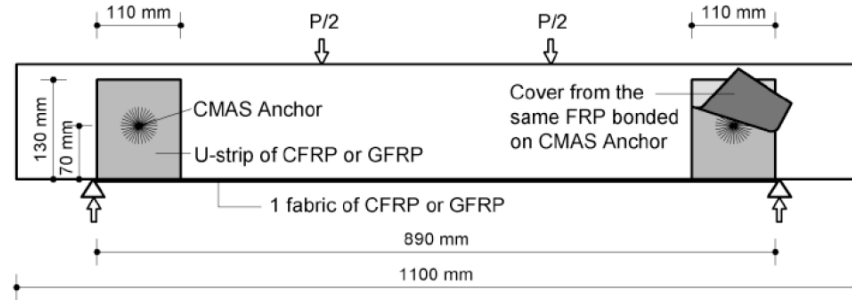


Figure 8. U-Wraps anchored with fiber anchors (CMAS anchors) (Demakos et al., 2013).

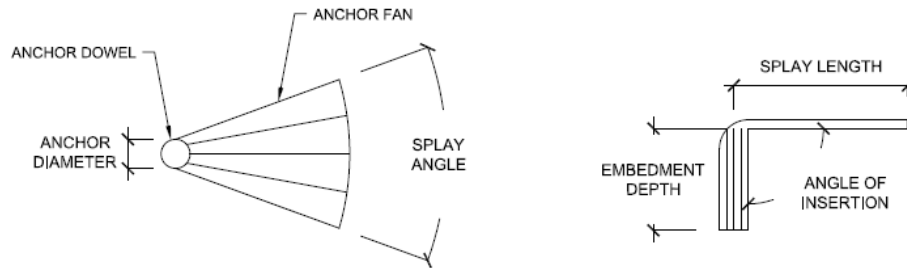
## FIBER ANCHORS

Research regarding anchorage for flexural FRP has mostly been confined to U-Wraps. U-Wraps consist of the same material and have the same installation process as the flexural CFRP; however, a large amount of a relatively expensive material is used to anchor the flexural CFRP. Therefore, researchers have explored different anchoring methods to suppress IC debonding. A common anchorage method that has been investigated to suppress IC debonding is fiber anchors (Figure 5b). Fiber anchors provide an appealing alternative to U-Wraps, as they use a minimal amount of carbon fiber when compared to U-Wraps. Additionally, fiber anchors can be used to anchor flexural CFRP on slabs, whereas U-Wraps cannot due to the fact that there are no vertical faces to turn up the carbon fiber reinforced polymer sheets.

Fiber anchors are made from either a bundle of fibers or rolled sheets of CFRP. A fiber anchor consists of two separate parts, the anchor dowel (embedded region) and the anchor fan. The saturated anchors are carefully placed through the woven fibers in the laminate and inserted into a hole drilled in the concrete member. The loose fibers in the anchor fan are then splayed over the laminate in the direction of the tensile forces. There is little knowledge regarding fiber anchor's effect on increasing the structural performance of concrete beams flexurally strengthened with CFRP. Fiber anchors still have multiple variables that have not been completely isolated during testing or explored at a structural scale. Some of these critical variables include splay length, splay angle, embedment depth, and the angle at which the anchor dowel is inserted into the concrete beam (angle of insertion) (Figure 9). The amount of fibers placed within a fixed diameter may vary from anchor to anchor. Therefore, it has been suggested to use the equivalent anchor area rather than the anchor diameter to define the size of a fiber anchor (Jirsa et al., 2017). The equivalent anchor area is the cross-sectional area the fibers in the fiber anchor would create as if it were a laminate sheet of CFRP. Since the anchor and the laminates are made from the same material, Jirsa et al. (2017) defined the equivalent anchor area using the weight of the strip laminate per surface area ( $\gamma_{s,Exp}$ ) and the weight of the anchor per unit length ( $\lambda_A$ ) as seen in Equation 1:

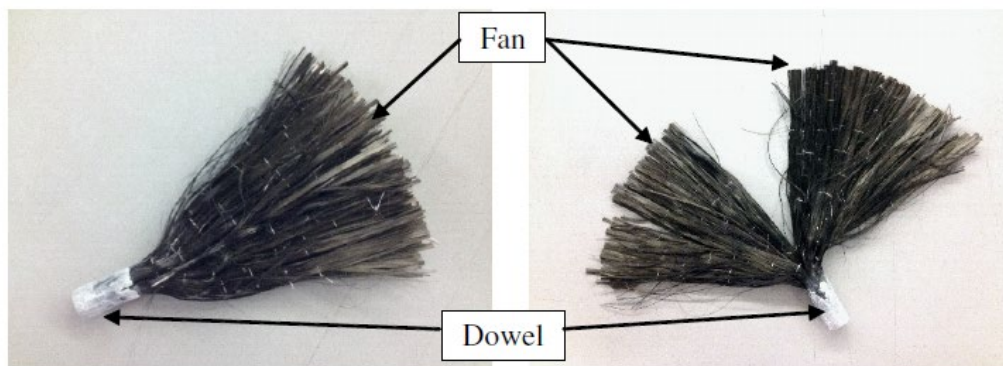
$$A_{Eqv} = \frac{\lambda_A}{w_f \gamma_{s,Exp}} (w_f t_f) \quad 1$$

where,  $w_f$  is the width of the CFRP strip and  $t_f$  is the total thickness of the CFRP strip.



**Figure 9. Fiber anchor variables.**

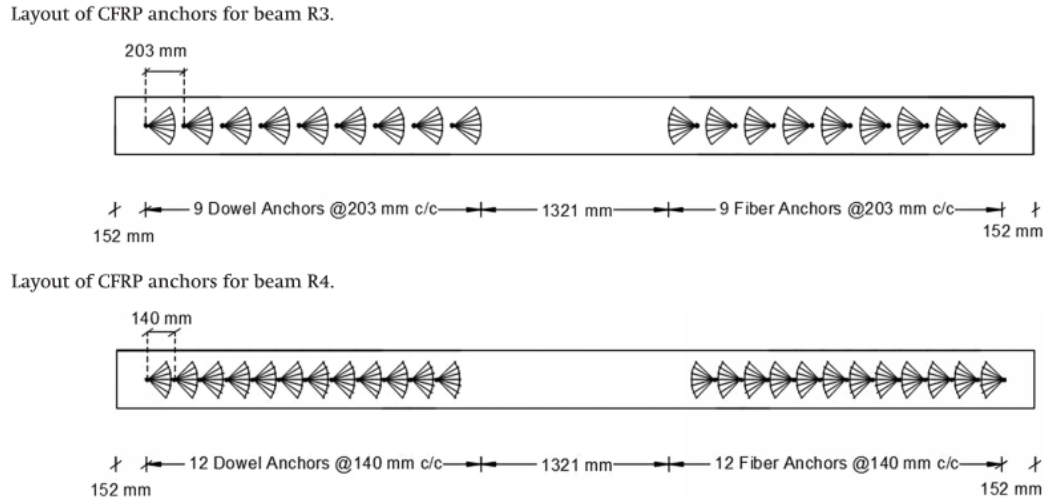
Figure 10 shows both a dry bow-tie and single-fan anchor. Both types of anchors produced similar results in both direct shear pull-off and structural-scale testing (Zhang & Smith, 2012, Smith et al., 2011). Bow-tie anchors were shown to provide slightly greater residual strength when compared to single-fan anchors. However, this comes as a result of using twice the equivalent anchor area (Zhang & Smith, 2012a). The fiber anchors enhance the bond between the flexural CFRP and the concrete member due to the fiber anchors reducing the interfacial normal stresses that are developed during the beam's deflection. Additionally, the embedment of the anchor allows the laminate to develop higher strains, up to 32% higher than unanchored specimens (Zhang & Smith, 2017).



**Figure 10. Dry single-fan (left) and bow-tie (right) fiber anchors (Smith et al., 2013).**

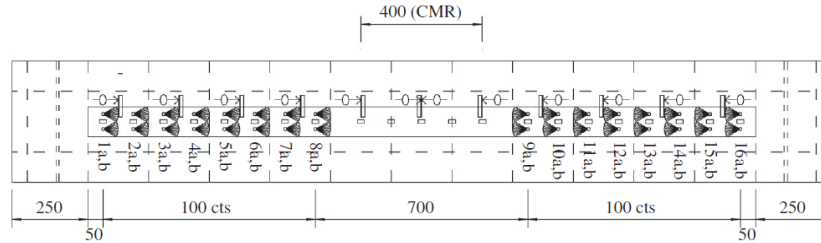
Studies have been conducted utilizing fiber anchors to delay IC debonding on structural-scale slabs (Smith et al., 2011; Smith et al., 2013). The authors explored variables related to the positioning and geometry of fiber anchors to enhance the load-carrying capacity and ductility of the reinforced concrete slabs. It was determined that anchors placed at the ends of the laminate can facilitate ductile slab behavior as well as increase the maximum load up to 36% compared to the unanchored control specimen (Smith et al., 2013). As previously discussed, a governing failure mode of unanchored flexural CFRP can be concrete cover delamination. Similar to U-Wraps, the placement of fiber anchors at the ends of the laminate can shift the governing failure mode away from end peeling and toward IC debonding (Smith et al., 2011; Smith et al., 2013).

The best utilization of the flexural CFRP in structural-scale testing occurred when anchorage was provided throughout the entire length of the shear span. Fiber anchors that were placed in the high moment region of the beam contributed little to the load-carrying capacity (Smith et al., 2011). Zaki & Rasheed (2019) showed that the load capacity of flexurally strengthened members was increased when the equivalent anchor area of the anchors was decreased and the number of anchors was increased (Figure 11). Beam R3 had a total of 18 anchors evenly spaced within its shear spans. Beam R4 had a total of 24 anchors evenly spaced within its shear spans and the equivalent anchor area of each anchor was decreased. The sum of the equivalent anchor areas were identical between Beams R3 and R4. Furthermore, the additional fiber anchors in Beam R4 allowed Zaki & Rasheed (2019) to position them such that the shear span was completely covered without any “free regions” between the anchors as seen in Beam R3 (Figure 11). The flexural capacity of Beam R4 increased by 4% compared to Beam R3 (14% compared to the unanchored test specimen) and was able to completely suppress IC debonding up to its failure by concrete crushing (Zaki & Rasheed, 2019). It was suggested that completely covering the shear span with anchorage restricted debonding of the laminate within the shear span, thus providing an increase in flexural capacity (Zaki & Rasheed, 2019).



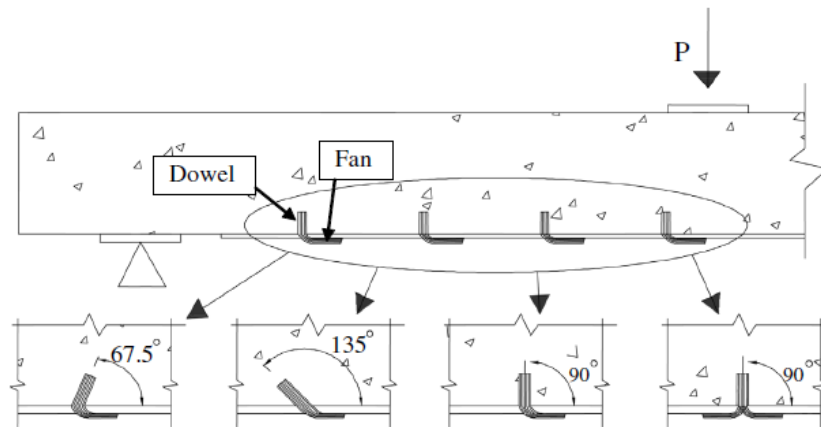
**Figure 11. Test iterations from Zaki & Rasheed (2019).**

Smith et al. (2013) completed a similar iteration between test specimens where 32 anchors were placed within the shear span of a slab (16 anchors per each half of the slab) (Figure 12). The ultimate load of the structural slab increased 44% compared to the unanchored control slab. The slab failed when the flexural CFRP ruptured at 95% of rupture strain reported in the study (Smith et al., 2013). The increase in load capacity of the structural slab can be accredited to the efficient transfer of forces from having transverse sets of anchors placed along the length of the laminate (Ozbakkaloglu et al., 2017; Smith et al., 2013). However, having to install 32 anchors to achieve optimal performance from the flexural CFRP is less than ideal due to the preparation and labor that is required during the fiber anchor installation process. A major appeal of using CFRP as a strengthening material is that repairs can be completed in a rapid manner. Therefore, it is recommended to explore other variables pertaining to fiber anchors, such as splay length or equivalent anchor area, to increase the load capacity and ductility of FRP-strengthened members.



**Figure 12. Test iteration from Smith et al. (2013).**

Studies have explored inserting the dowels of the fiber anchors at angles other than perpendicular into the beam (Figure 13). Small-scale direct shear pull-off testing investigated the angle of insertion of the anchor dowel relative to the direction of the tensile load. It was found that increasing the angle of insertion can result in maximum tensile loads as much as 24% greater than an identical fiber anchor installed at 90 degrees (Zhang & Smith, 2012b). This is likely due to the angle of insertion reducing the stress concentration at the transition between the anchor dowel and anchor fan (Kalfat et al., 2018). The improved performance of fiber anchors installed at an angle has also been confirmed on a structural scale. Increasing the angle of insertion of fiber anchors on a structural-scale slab resulted in an increase of the maximum strain in the laminate of 18% (Smith et al., 2013).

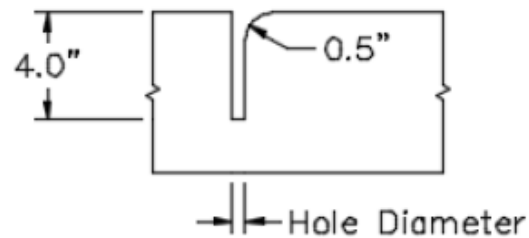


**Figure 13. Angle of insertion (Smith et al., 2013).**

Direct shear pull-off testing was utilized to investigate the ratio between the splay diameter and the equivalent anchor area. Anchors with larger splay length appeared to engage larger regions of the laminate, which requires a load resistance from the anchors. Therefore, it was hypothesized that the splay length of the anchor should be determined upon the width of the anchor, as it limits the anchor's capacity (Niemitz et al., 2010). Increasing the splay length of the anchors was shown to increase the maximum load and strain of the longitudinal CFRP. By nearly doubling the splay length, the average maximum load increased by 8% in small-scale beam testing (Jirsa et al., 2017).

The University of Texas at Austin (UT Austin) has conducted small-scale testing on flexurally strengthened concrete beams (Jirsa et al., 2017). Multiple techniques were utilized during the installation of their fiber anchors, which were intended to improve the load capacity of fiber anchors installed on flexural CFRP. It was recommended to make the diameter of the anchor hole 1.4 times larger than the diameter of the fiber

anchor to facilitate the placement of the fiber anchor into the concrete. Additionally, the edges of the hole diameter should be rounded to a  $\frac{1}{2}$  in. radius (Figure 14). This helps to reduce stress concentrations at the transition from the anchor dowel to the anchor fan which can contribute to anchor rupture (Jirsa et al., 2017). It has also been recommended to place a sheet of FRP over the splay of the anchor. It was suggested that “sandwiching” the anchor between plies of the flexural CFRP eases the transfer of load from the flexural CFRP to the anchor (Jirsa et al., 2017).



**Figure 14.**  $\frac{1}{2}$ " fillet at the edge of the anchor hole (Jirsa et al., 2017).

The introduction of fiber anchors to concrete beams flexurally strengthened with CFRP can mitigate concrete cover delamination and increase the ultimate load capacity of the beam. Once debonding of the laminate begins to propagate, the load placed on the fiber anchors increases. The increase in load typically results in the partial or complete rupture of the fiber anchors (Zhang et al., 2012). Fiber anchors usually rupture at the transition between the anchor dowel and the anchor fan. This 90-degree bend creates a stress concentration in the anchor, which can ultimately lead to the anchor’s failure. The anchors placed closest to the high moment region typically fail first, as the anchors have been shown to develop higher post debonding loads than anchors placed further away from the high moment region (Ozbakkaloglu et al., 2016). As previously stated, the diameter of the anchor hole should be chamfered to help reduce the stress concentrations developed at the 90-degree bend. Structural-scale testing has shown that the rupture of the flexural CFRP can occur when the fiber anchors can resist the loads placed on the anchors during the debonding of the flexural CFRP (Smith et al., 2013). It should be noted that isolated anchors can still rupture prior to the rupture of the laminate, as seen in Smith et al. (2013).

## KNOWLEDGE GAPS

It has been established that both U-Wraps and fiber anchors are anchorage methods that can suppress end peeling and delay IC debonding, thus enhancing the utilization of the flexural CFRP. In fact, the presence of U-Wraps or fiber anchors has resulted in the laminate reaching its rupture strain in multiple studies (Smith et al., 2013; Yalim et al., 2008; Breña et al., 2003; Hasnat et al., 2016; Rasheed et al., 2015). Although the maximum utilization of the laminate has been achieved, there is still an inconclusive knowledge of how fiber anchors and U-Wraps affect the performance of a concrete member flexurally strengthened with CFRP. Attempts have been made to create an objective model to predict the shear capacity of U-Wraps as flexural anchors. A rational design model created by Raheem & Rasheed et al. (2021) was developed based on simple mechanics of materials to compute the capacity of U-Wraps anchors on flexural CFRP. When U-Wraps are evenly distributed along the girder’s shear span, an increase to the debonding strain of the longitudinal CFRP may be applied based on the number of U-Wraps. While this model was supported in Raheem & Rasheed et al. (2021), further research should be conducted to confirm that this design approach is universally applicable.

U-Wraps placed in the shear span of the beam were shown to provide the greatest increase in load-carrying capacity. Fu et al. (2018) showed that increasing the width of the U-Wraps placed in the shear span can increase the load-carrying capacity of the concrete beam. Increasing the width of the U-Wrap from 100-mm to 150-mm resulted in an increase of load capacity of 14% (Fu et al., 2018). U-Wraps covering the entire width of the shear span was observed to be the optimal width of the U-Wraps in a small-scale study. Providing U-Wraps at this width can result in an increase of the load-carrying capacity as much as 97% compared to the unanchored control beam (Hasnat et al., 2016). Additionally, increasing the thickness of the U-Wraps can result in additional load-carrying capacity of the concrete beam. A study completed by Hasnat et al. (2016) showed that increasing the thickness of the U-Wraps from one to two plies increased the load-carrying capacity of the beam an average of 16% between each of their U-Wrap configurations. Lastly, multiple studies have shown that orienting the fibers of U-Wraps placed at the ends of the laminate at 45 degrees has resulted in increased performance compared to 90-degree U-Wraps. When the U-Wraps are oriented at 45 degrees, increases in maximum load have been observed to be as much as 52% and 60% as compared to 90-degree U-Wraps of a similar width (Sagawa et al., 2001; Fu et al., 2018).

Although a majority of the variables regarding U-Wraps have been explored in small-scale experiments, a working knowledge of how U-Wraps affect the structural performance of a flexural member strengthened with CFRP is still developing. The effect each variable has on the load capacity and ductility of a strengthened flexural members still needs to be further examined to understand which variables have a larger effect than others (i.e., U-Wrap placement, U-Wrap thickness, etc.). This will help develop design guidelines for how U-Wraps should be installed on strengthened beams and girders as flexural anchors. Additionally, more accurate models may be developed that account for how U-Wraps affect the performance of a flexural strengthened member.

Fiber anchors are an appealing alternative to U-Wraps as a means of flexural anchorage. Fiber anchors use a minimal amount of a relatively expensive material as compared to U-Wraps. Additionally, fiber anchors can be used to anchor flexural CFRP on concrete slabs, whereas U-Wraps cannot be used, since there is no vertical face to turn up the transverse sheets of CFRP. Direct shear pull-off testing has shown that providing fiber anchors can develop strains in the flexural CFRP up to 32% higher than unanchored specimens (Zhang & Smith, 2017). Introducing fiber anchors to structural-scale reinforced concrete slabs flexurally strengthened with CFRP has resulted in the rupture of the laminate and concrete crushing, yielding the optimal utilization of the laminate (Smith et al., 2013; Zaki & Rasheed, 2019). Furthermore, the presence of fiber anchors can lead to an increase of maximum load up to 44% as compared to the unanchored slabs (Smith et al., 2013).

Multiple variables regarding fiber anchors have only been explored in small-scale or direct shear pull-off studies. A study conducted by UT Austin showed that increasing the anchor area or splay length can result in an increase of the average load-carrying capacity of small-scale beams (Jirsa et al., 2017). Smith et al. (2011) and Smith et al. (2013) experimented with varying anchor areas in their structural-scale studies. However, this variable was not completely isolated in testing. Therefore, the effect that the fiber anchor area and splay length have on the performance of a structural-scale concrete flexural member is still unclear. Other variables that have not been explored on structural-scale testing are the splay angle of the fibers and splay length of the anchor.

The ratio between the amount of anchorage, whether it be U-Wraps or fiber anchors, to the amount of flexural CFRP provided on a concrete beam has not been explored on a structural scale. Specifically, we are referring to the effect this ratio has on the load capacity and ductility of a strengthened flexural member.

Exploring this ratio may help to estimate the increase in load capacity or ductility of a strengthened reinforced concrete beam based on the area of anchorage added to the flexural CFRP.

Furthermore, the interaction that strain hardening and anchorage has on the increase in load capacity has not been explored. Reinforced concrete beams can fail by cover delamination or IC debonding before the steel reinforcement reaches strain hardening. The increase in load capacity has strictly been viewed as a result of the addition of anchorage to the CFRP. However, due to the assumption of elastic perfectly-plastic steel reinforcement in concrete beam design, a portion of the increase in load capacity comes from the strain hardening behavior of the concrete beam. Ultimately, the increase in load capacity due to the addition of anchorage should be isolated from the strain hardening behavior to account for the increase in load capacity solely due to the addition of CFRP and anchorage to a beam or girder.

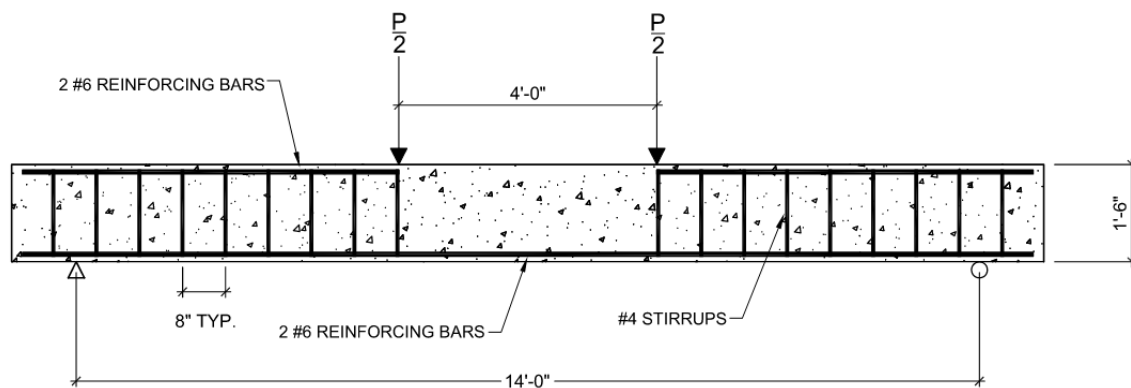
An objective of this study is to address the existing knowledge gaps of U-Wraps in structural-scale testing. The results from the structural-scale testing will help to develop a greater knowledge of how flexural anchors affect the load capacity and ductility of reinforced concrete girders flexurally strengthened with CFRP.

## CHAPTER 3

# Design and Construction of Specimens

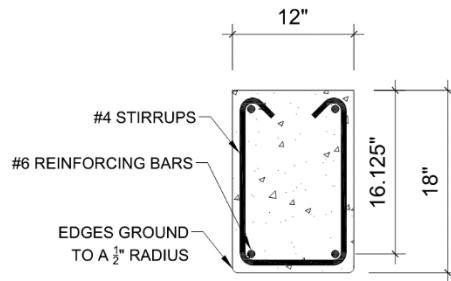
### DESIGN OF REINFORCED CONCRETE GIRDERS

This experimental program consisted of 12 reinforced concrete girders that were tested in four-point flexure. Each girder had a length of 16 ft with a clear span of 14 ft (Figure 15). The girders had a width of 12 in. and a depth of 18 in. The cross-section of the girder can be seen in Figure 16. The steel reinforcement of the girders consisted of two #6 longitudinal bottom reinforcing bars ( $\rho_s = 0.0045$ ) along with open #4 stirrups bent by the manufacturer of the reinforcing steel. The stirrups were placed at 8 in. on-center ( $\rho_v = 0.0042$ ) within the 6-ft shear spans of the girder. Additional #6 bars were placed on the top of the shear region of the girder to secure the rebar cage created by the stirrups. The reinforcement layout of the reinforced concrete girders is shown in Figure 15 and Figure 16. The girders were purposely designed to be lightly reinforced to exceed the minimum required longitudinal reinforcement ratio of 0.0033 provided by ACI Committee 318 (2019); this ensured a ductile failure mode of the unstrengthened reinforced concrete girder. This allowed for large increases in strength due to the addition of flexural CFRP to the girders without experiencing an undesirable failure of the girder by concrete crushing.



**Figure 15. Reinforcement layout of the girder.**





**Figure 16. Cross-section of the reinforcement layout of the girder.**

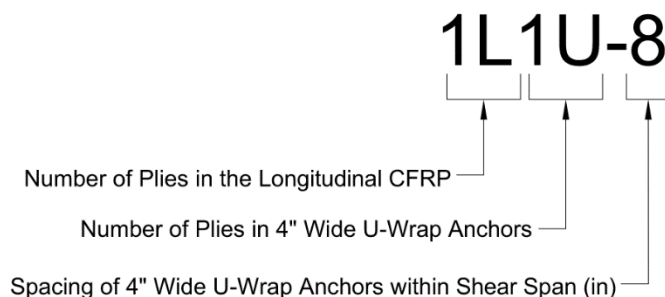
## DESIGN OF STRENGTHENED REINFORCED CONCRETE GIRDERS

A unidirectional carbon fiber reinforced polymer, Fyfe Tyfo SCH-41, was used to strengthen each of the reinforced concrete girders in flexure. Sheets of CFRP were installed along the tension face of the girder at a 10-in. width. The first sheet of CFRP spanned the entire length of the tension face of the girder and was terminated at the face of the support plates. Subsequent second and third plies were terminated 6 in. prior to the ends of the previous ply as recommended in ACI Committee 440 (2017) to avoid stress concentrations at the ends of the laminate, which contribute to end peeling as a failure mode. Figure 18 shows how CFRP was installed on each of the strengthened girders.

Given that the objective of this study was to investigate U-Wraps as flexural anchors, multiple variables pertaining to the design of the U-Wraps were considered. These include spacing of the U-Wraps, height of the U-Wraps, cross-sectional area of the U-Wraps, and cross-sectional area of the longitudinal CFRP. Ultimately, the relationship between the area of anchorage to the area of flexural CFRP was investigated to create an approach for flexural anchor design.

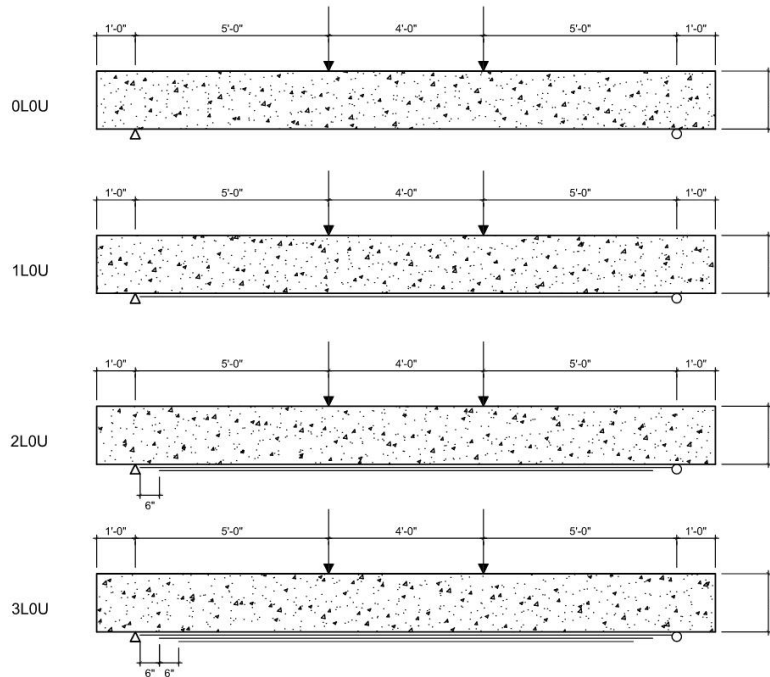
### Test Matrix

Figure 17 shows the girder nomenclature used in this study. The first term indicates the number of longitudinal plies of CFRP added to the girder. The second term indicates the number of plies of the 4 in. wide U-Wraps used as flexural anchorage. The final term is the center-to-center spacing of the U-Wraps within each of the shear spans expressed in inches. For example, the 1L1U-8 girder would have 1-ply of longitudinal CFRP and 1-ply of 4-in.-wide U-Wraps placed at 8 in. on-center within each of the shear spans.



**Figure 17. Example of the nomenclature used for the girders.**

Out of the 12 girders, 4 were used as control specimens. A plain reinforced concrete girder, 0L0U, was first tested as a benchmark for the remaining specimens strengthened with CFRP. The other three control girders were tested with 1, 2, and 3 longitudinal plies of CFRP without additional anchorage. They are herein referred to as 1L0U, 2L0U, and 3L0U, respectively. Figure 18 shows the control girders used in the study.



**Figure 18. Control girders used in the study.**

The remaining eight girders were strengthened flexurally with 1, 2, or 3 plies of CFRP and then anchored with U-Wraps. The same material used in the flexural laminate, Tyfo SCH-41, was used to create the U-Wrap anchors. The height and width of the U-Wraps remained constant throughout each of the eight girders anchored with U-Wraps. The U-Wraps did not extend the full height of the girder to account for the fact that slabs are typically integrated into concrete beams and girders. The U-Wraps had a height of 14 in., which is terminated 4 in. from the extreme compression fiber of the girders. Furthermore, the U-Wraps had a constant width of 4 inches. The quantity of the longitudinal CFRP, quantity of the U-Wraps, and the spacing of the U-Wraps within the shear span varied among the girders to investigate the relationship between the area of anchorage provided to the area of flexural CFRP.

The relation between the area of U-Wraps to the area of longitudinal CFRP was first compared using the equivalent longitudinal reinforcement ratio. The equivalent longitudinal reinforcement ratio, considering both internal steel reinforcement and CFRP, was defined as:

$$\rho_{\text{equiv}} = \frac{A_s}{bd} + \frac{nA_f}{bh} \quad 2$$

where  $A_s$  is the cross-sectional area of internal steel reinforcement;  $A_f$  is the cross-sectional area of longitudinal CFRP laminate;  $n$  is the ratio of modulus of elasticity of CFRP to that of steel; and  $b$ ,  $d$ , and  $h$

are concrete cross-section width, effective depth of the steel reinforcement, and total depth of the beam, respectively.

The quantity of U-Wraps applied to a given girder was quantified by  $A_{prov}$ :

$$A_{prov} = 2n_U t_U w_U \quad 3$$

where  $n_U$  is the number of U-Wraps within one of the shear spans of the girder;  $t_U$  is the thickness of the CFRP used in the U-Wraps; and  $w_U$  is the width of each U-Wrap.  $A_{prov}$  is the total cross-sectional area of the U-Wraps within a shear span of a girder. The leading factor “2” takes into consideration both legs of a U-Wrap.

$A_{prov}$  was normalized to the cross-sectional area of a U-Wrap that is to be placed at the ends of a flexural CFRP laminate to mitigate end debonding as a failure mode (per ACI Committee 440, 2017):

$$A_{fanchor} = \frac{(A_f f_{fe})_{longitudinal}}{(E_f \kappa_v \epsilon_{fe})_{anchors}} \quad 4$$

where  $A_f$  and  $f_{fe}$  are the cross-sectional area and the effective stress of the flexural CFRP, respectively;  $E_f$  is the elastic modulus of the CFRP used for the U-Wraps;  $\kappa_v$  and  $\epsilon_{fe}$  are the bond reduction coefficient (specified in ACI Committee 440 2017) and the effective strain of the U-Wraps, respectively.

The relationship of the area of U-Wraps provided to the area of flexural CFRP provided was quantified by the ratio of  $A_{prov}$  to  $A_{fanchor}$ , herein referred to as the anchorage ratio. The values of  $A_{prov}$ ,  $A_{fanchor}$ , and the anchorage ratio are shown in Table 1 for all girders. Among the girders tested with U-Wraps, a range of anchorage ratios of 1.20 to 2.45 was obtained to investigate the anchorage ratio. Figure 19 shows the U-Wrap configurations for each of the girders flexurally strengthened with CFRP and anchored U-Wraps, and Figure 20 shows the numeric labels used to denote each of the U-Wraps on the girders.

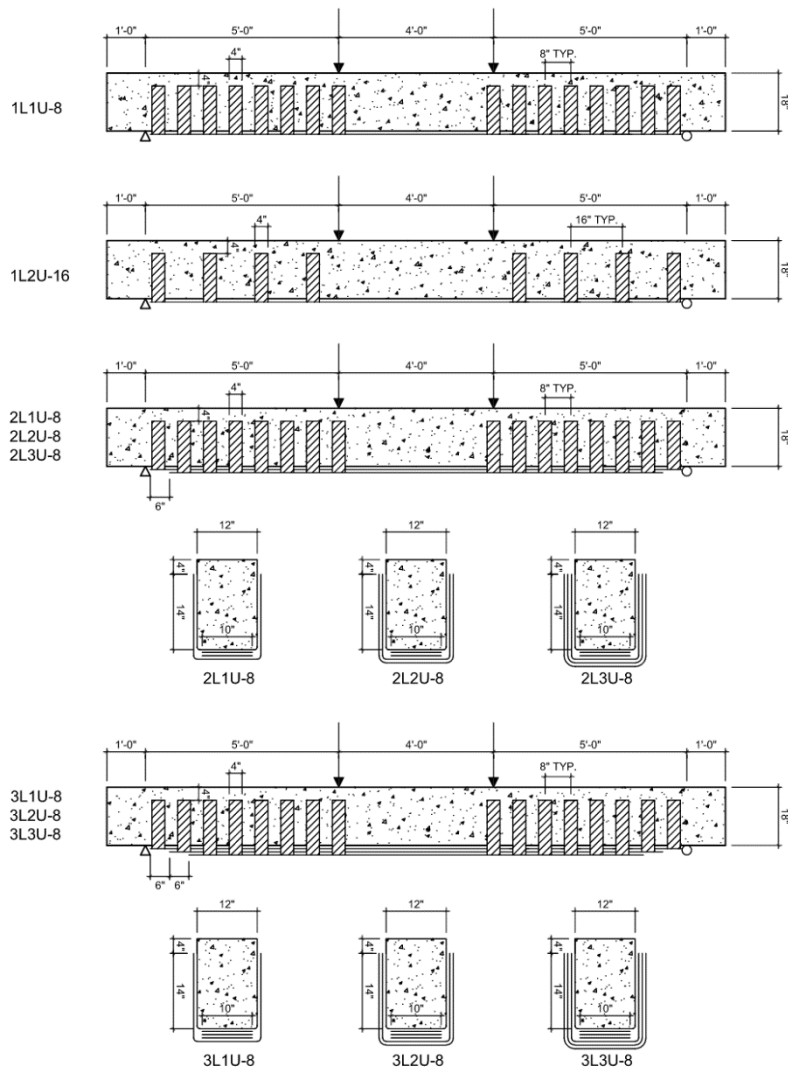
**Table 1. Anchorage ratios for each of the 12 girders.**

<b>Girder</b>	<b>A<sub>f</sub></b> <b>(in<sup>2</sup>)</b>	<b>A<sub>vf</sub></b> <b>(in<sup>2</sup>)</b>	<b>ρ<sub>equiv</sub></b> <b>(%)</b>	<b>A<sub>prov</sub></b> <b>(in<sup>2</sup>)</b>	<b>A<sub>fanchor</sub></b> <b>(in<sup>2</sup>)</b>	<b>A<sub>prov</sub> / A<sub>fanchor</sub></b>
0L0U	-	-	0.45	-	-	-
1L0U	0.40	-	0.54	-	-	-
1L1U-8	0.40	0.16	0.54	2.56	1.23	2.08
1L2U-16	0.40	0.32	0.54	2.56	1.77	1.45
2L0U	0.80	-	0.63	-	-	-
2L1U-8	0.80	0.16	0.63	2.56	1.74	1.47
2L2U-8	0.80	0.32	0.63	5.12	2.51	2.04
2L3U-8	0.80	0.48	0.63	7.68	3.13	2.45
3L0U	1.20	-	0.72	-	-	-
3L1U-8	1.20	0.16	0.72	2.56	2.13	1.20
3L2U-8	1.20	0.32	0.72	5.12	3.07	1.67
3L3U-8	1.20	0.48	0.72	7.68	3.83	2.00

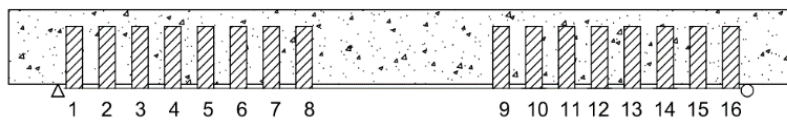
A<sub>f</sub>: cross-sectional area of longitudinal CFRP laminate

A<sub>vf</sub>: cross-sectional area of each U-wrap laminate

ρ<sub>equiv</sub> : equivalent reinforcement ratio



**Figure 19. Test matrix of flexurally strengthened girders with U-Wrap anchorage.**



**Figure 20. Numeric labels used to denote U-Wraps spaced at 8 in. on-center. U-Wraps 1, 3, 5, 7, 10, 12, 14, and 16 were used on the girder with U-Wraps spaced at 16 in. on-center (1L2U-16).**

## CFRP INSTALLATION

### Surface Preparation

Prior to the installation of CFRP on the girders, each of the girders underwent surface preparation. The CFRP manufacturer, Fyfe, recommends an International Concrete Repair Institute (ICRI) concrete surface profile of 2 to 3 prior to the installation of the CFRP (International Concrete Repair Institute, 2013). The purpose of surface preparation is to create a rough surface to enhance the mechanical interlock between the adhesive and concrete substrate. In addition, surface preparation removes dirt and oils, reveals air pockets, and removes unsound concrete that may interfere with the bond of the CFRP to the concrete substrate. Each of the girders strengthened with CFRP had its surface prepared to a concrete surface profile of 3 using abrasive blasting (or sand blasting). International Concrete Repair Institute (2013) outlines the selection and methods for surface preparations of concrete for coatings, sealants, polymer overlays, and concrete repairs. To achieve a concrete surface profile of 3, it is recommended to use light abrasive blasting. Furthermore, abrasive blasting is a method of surface preparation that will not introduce micro-cracking into the surface of the concrete, which may negatively impact the CFRP bond.

The concrete substrate of each of the strengthened girders was prepared via abrasive blasting at the University of Delaware Structures Laboratory. A 110-lb capacity, 20-gal abrasive pressure blaster provided by the manufacturer, Allsource, was used for the surface preparation with Black Diamond Coal Slag 2040 as the abrasive media. ICRI rubber concrete surface profile coupons were used to ensure that the concrete substrate met a concrete surface profile of 3 (Figure 21).



**Figure 21. Confirming the CSP of the concrete using an ICRI surface profile coupon.**

Studies have shown that stress concentrations form in U-Wraps at the 90-degree transition between the tension face and vertical faces of a girder (Lee & Lopez, 2016). Therefore, the corners of the girder were cast with a ½-in. wooden chamfer. The corners of the girders were additionally ground using a masonry grinding wheel to create a smooth ½-in. radius to further reduce the stress concentrations at the 90-degree bend in the U-Wraps (Figure 22).



**Figure 22. Typical ground edge of a girder.**

## **CFRP Installation**

The CFRP application surfaces were first cleaned with compressed air to remove any debris (Figure 23). The Part A and Part B components of the epoxy were mixed at the manufacturer's recommended weight ratio of 100 Part A to 34.5 Part B. A scale was used to properly weigh out the desired proportions (Figure 24). The Part A and Part B components were added to a 5-gallon bucket and were mixed with a paddle drill mixer at a speed of approximately 500 rpm until the epoxy was uniformly blended (Figure 25). An epoxy primer coat was then applied to the concrete substrate using an epoxy roller to create surface saturated-dry conditions of the concrete substrate (Figure 26). The epoxy was applied to the tension face and each of the vertical faces of the girders. Thickened epoxy was used prior to the application of the CFRP to level the surface of the concrete as well as to fill any large voids that were observed in the concrete substrate. The predetermined amount of the epoxy mixture was removed and placed into a separate 5-gallon bucket to make the thickened epoxy by mixing fumed silica and epoxy. Using a paddle drill mixer, the thickened epoxy was mixed at a speed of approximately 500 rpm until it was uniformly blended. The thickened epoxy was applied onto the surface of the girder using plastic putty knives (Figure 27 and Figure 28). Thickened epoxy was applied atop of epoxy primer where flexural CFRP and U-Wraps were bonded to the concrete substrate. Care was taken to fill all larger voids and bugholes in the concrete with the thickened epoxy.



**Figure 23. Cleaning the surface of the concrete with compressed air.**



**Figure 24. Measuring the weight of the Part A component of the epoxy.**



**Figure 25. Mixing the epoxy in a 5-gallon bucket using a paddle drill mixer.**

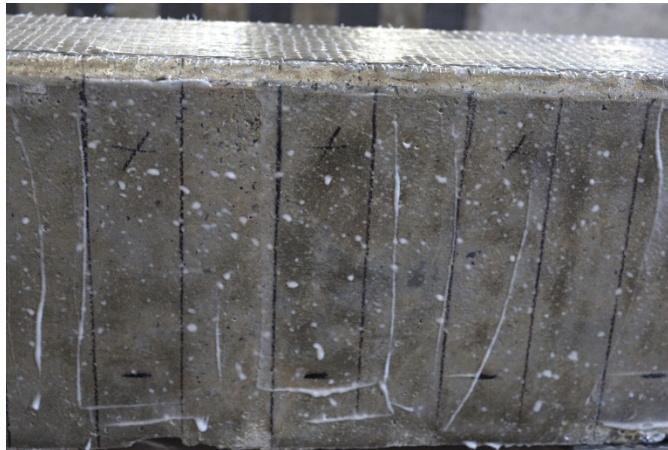


**Figure 26. Applying epoxy to the concrete substrate using an epoxy roller.**





**Figure 27. Applying thickened epoxy to the tensile face of the girder using a plastic putty knife.**



**Figure 28. Thickened epoxy applied to the vertical face of the girder at the locations of the U-Wraps.**

The CFRP was saturated with the epoxy at a one-to-one weight ratio of the CFRP to the weight of the epoxy. An epoxy bath was created with plastic sheeting on an elevated surface to saturate the CFRP. The CFRP was laid on the plastic sheeting of the epoxy bath where the epoxy was then added to the dry fibers. The epoxy was spread evenly across the dry fibers using a plastic putty knife as well as an epoxy roller (Figure 29). This process was completed once for each side of the CFRP sheet to ensure the sheet was properly saturated throughout its thickness. Once the CFRP was saturated, it was ready to be installed on the girder. The longitudinal sheets were rolled onto a section of PVC pipe while still in the epoxy bath (Figure 30). The CFRP sheet was then transferred to the surface of the girder, where it was rolled off the PVC pipe (Figure 31). Once the longitudinal CFRP was transferred to the girder, the sheet was smoothed with a plastic putty knife to further distribute epoxy, ensure the CFRP was installed firmly against the concrete substrate to remove any air voids between the concrete and CFRP and level the surface of the CFRP (Figure 32). The U-Wraps were installed perpendicular over the longitudinal CFRP and then smoothed onto the surface of the girder by hand (Figure 33).



**Figure 29. Spreading epoxy on the dry fibers using a putty knife within the epoxy bath.**



**Figure 30. Rolling the saturated fiber onto a section of PVC.**



**Figure 31. Installing the longitudinal sheet of CFRP onto the tensile face of the girder.**



**Figure 32. Smoothing the CFRP onto the surface of the beam using a putty knife.**



**Figure 33. Installing U-Wraps onto the girder.**

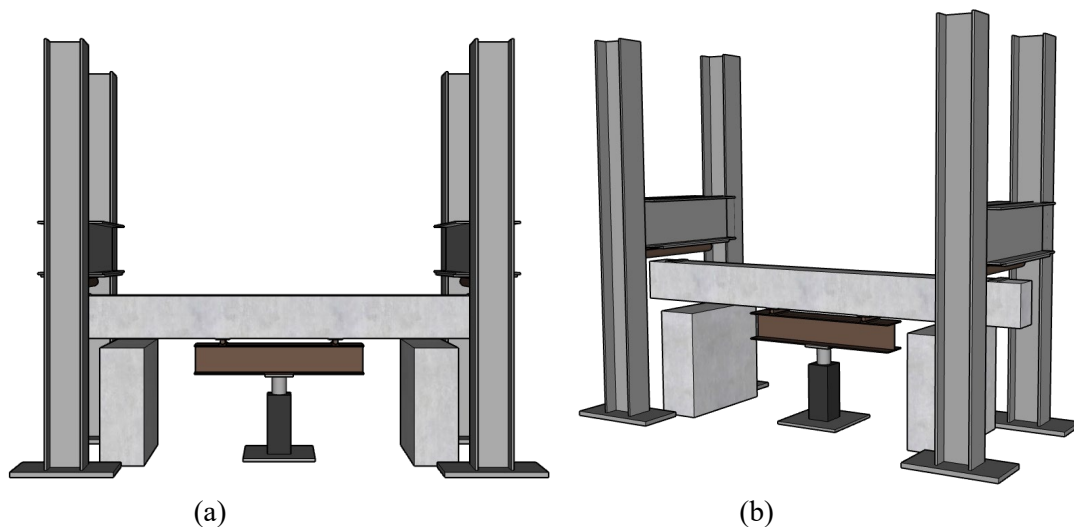
## CHAPTER 4

# Experimental Test Setup

### TEST SETUP

Each of the 12 reinforced concrete girders were tested in the Structural Engineering Laboratory at the University of Delaware. The girders were simply supported and tested in an inverted position via four-point bending. A 3D digital image correlation (DIC) system was used to measure full-field displacements on the girder surface facing the cameras. The girders were inverted to ensure that the DIC system could capture the entire girder within its field of view (Figure 34 and Figure 35).

The load was applied to the girder through a 150-kip hydraulic actuator. The 150-kip hydraulic actuator was attached to a 30 in. x 30 in. x 2 in. thick steel plate that was then welded to the strong floor. The hydraulic actuator was connected to an MTS system controller, where the load was applied under displacement control of 0.15 mm/s. A 6-ft spreader beam was attached to the load cell on the actuator to distribute two-point loads, creating a constant moment region of 4 ft within the center of the girder. Steel plates measuring 12 in. x 6 in. x 1/2 in. thick were placed under the loading points to distribute the load onto the girder. Furthermore, 10 in. x 4 in. x 1/2 in. thick steel plates were placed at the supports. The columns of the test frame were set 14 ft apart and the supports were welded between the columns. The girder was rested on concrete blocks within the test frame to support the girder between the tests. This resulted in the actuator having to lift the girder approximately 1 1/2 in. to reach the supports and load the girder.



**Figure 34. 3D diagrams of the test setup: (a) elevation view of the test setup; (b) isometric view of the test setup.**



**Figure 35. Photographs of the test setup: (a) elevation view of the test setup; (b) wide shot of the test setup.**

### THREE-DIMENSIONAL DIGITAL IMAGE CORRELATION SYSTEM

As previously stated, a 3D DIC system, Aramis by the manufacturer gom, was used during each of the flexural tests of the girders. The DIC system consists of two cameras with 12-mm lenses placed on a 6 ½-ft aluminum bar where the distance between the cameras can be modified. The distance between the cameras on the 6 ½-ft bar is determined by the distance to the object that is being tested, the desired field of view, and the angle of the cameras. The cameras and the 6 ½-ft bar were placed on top of a 14-ft aluminum column to ensure the entire girder was within the field of view of the cameras and that the proper distance between the cameras and the girder was achieved (Figure 36a). The angle of the cameras relative to the girder remained at the manufacturer-recommended 25 degrees. The column was placed approximately 10 ½ ft from the center of the girder to achieve the desired 14-ft distance between the cameras and the girder. The cameras and the 6 ½-ft bar were angled downwards using pan-tilts to capture both the tension face of the girder as well as the vertical face within the field of view of the cameras (Figure 36b).



**Figure 36. Photographs of the DIC system test (red arrows showing DIC cameras): (a) DIC system placed on top of the aluminum column; (b) test setup with the DIC system (red arrows showing DIC cameras).**

Prior to placing the DIC system on the aluminum column, the DIC system had to be calibrated. The calibration process required the use of a 7¾-ft calibration cross provided by the product manufacturer (Figure 37). Multiple images of the calibration cross at differing pre-determined angles, distances, and locations were taken to complete the calibration process.



**Figure 37. Calibration cross used for the DIC system.**

To capture full-field displacements of the girder, a contrasting speckled pattern was applied to the girder. The tension face and one of the vertical faces of the girders were first spray painted using a flat white paint. Then a black speckle pattern was applied over the white paint using a brush. The black speckle pattern was applied until approximately 50-50 coverage was achieved (Figure 38). Due to the speckled pattern, the DIC system was able to track displacements of the speckles during the loading of the girders and create a finite element mesh over the surface of the girders. Ultimately, this allowed the DIC system to calculate displacements and strains along the length of the girder. The finite element mesh created on each of the girders was adjusted such that an average distance between nodes on the triangular mesh was approximately 2 in.



**Figure 38. Speckled pattern applied to the vertical and tension faces of the girder.**

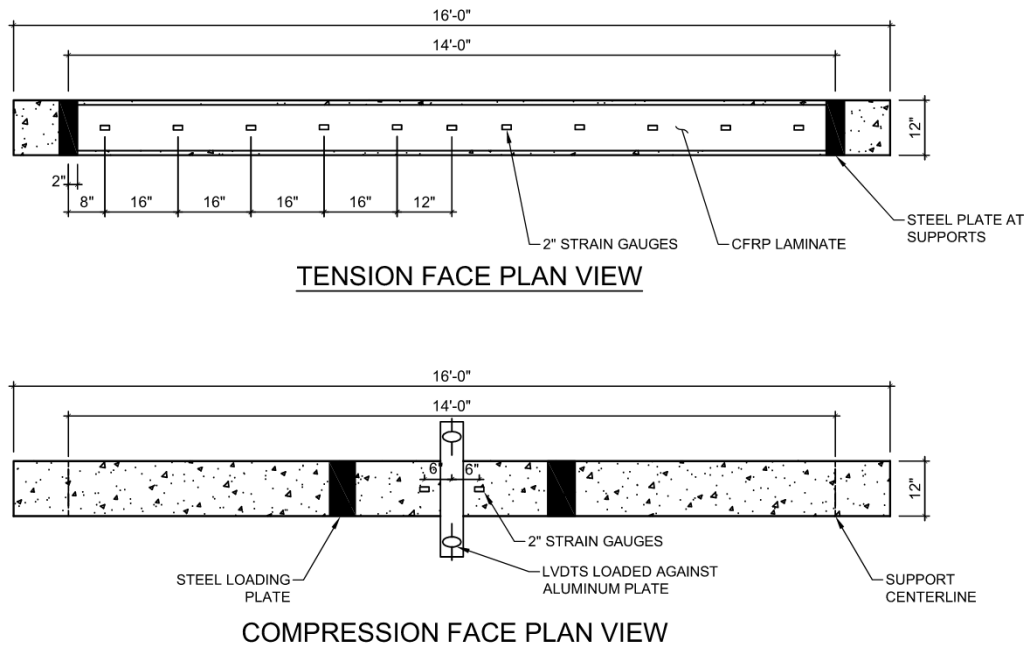
## **GIRDER INSTRUMENTATION**

In addition to the DIC system, hard instrumentation was also incorporated into the test setup. On the tension face of the girders, 2-in.-long uniaxial electrical resistance strain gauges were placed on the CFRP. The strain gauges were from the manufacturer Kyowa Electronic Instruments Co., Ltd. and had a resistance of

120 ohms. The strain gauges were placed at 16 in. on-center within each of the shear spans and approximately 12 in. on-center within the constant moment region. On the compression face of the girders, a ½-in.-thick aluminum plate was adhered to the girders at midspan. The aluminum plate extended on each side of the girder. Two spring-loaded linear variable differential transformers (LVDTs) by the manufacturer RDP Electronics Ltd. were placed against the aluminum plate at each end to measure midspan displacements (Figure 39). Furthermore, two 2-in. strain gauges were placed 6 in. offset on each side of the aluminum plate to measure compressive strains at the concrete surface. Figure 40 shows the typical layout for the girder instrumentation.



**Figure 39. LVDT loaded against the aluminum plate adhered to the girder.**



**Figure 40. Typical instrumentation plan of a girder.**

## CHAPTER 5

# Characterization of Materials Properties

### CONCRETE MATERIAL PROPERTIES

The reinforced concrete girders were placed from two separate ready-mix concrete trucks provided by Heritage Concrete. The first truck, Truck 1, was used to place girders 0L0U, 1L1U-8, 1L2U-8, 2L1U-8, 2L2U-8, and 2L3U-8. The second truck, Truck 2, was used to place girders 1L0U, 2L0U, 3L0U, 3L1U-8, 3L2U-8, and 3L3U-8. Each truck contained the same ready-mix concrete design provided by the manufacturer. The concrete mix design consisted of a 4,000-psi air-entrained concrete (Table 2).

*Table 2. Concrete mix design.*

Material Type	ASTM	Design Quantity	Truck 1 Batch Weights	Truck 2 Batch Weights
		per yd <sup>3</sup>	per yd <sup>3</sup>	per yd <sup>3</sup>
Cement	C-150	560 lb.	572 lb.	558 lb.
Coarse Aggregate	C-33	1780 lb.	1780 lb.	1780 lb.
Fine Aggregate	C-33	1340 lb.	1390 lb.	1410 lb.
Air Entraining Admixture	C-260	28.0 lq oz./yd <sup>3</sup>	28.0 lq oz./yd <sup>3</sup>	28.0 lq oz./yd <sup>3</sup>
Water Reducing Admixture	C-494	1.23 lq oz./yd <sup>3</sup>	1.23 lq oz./yd <sup>3</sup>	1.54 lq oz./yd <sup>3</sup>
Water	C-1602	30.5 gal	30.4 gal	29.4 gal.
Water-to-Cementitious Materials Ratio	C-1602	0.450	0.450	0.446

The concrete from each truck was sampled and tested onsite for laboratory testing of its material properties. For each truck, eighteen 4 in. x 8 in. cylinders and twelve 6 in. x 6 in. x 20 in. beams were molded per ASTM C31 for compressive and flexural strength testing, respectively (Figure 41 and Figure 42). Furthermore, the slump, temperature, unit weight, and air-content of the concrete were taken at the time of placement for each of the trucks. Table 3 shows the results from each of the field tests along with the corresponding testing method that was followed.





**Figure 41. Filling concrete into 4 in. x 8 in. cylinder molds.**



**Figure 42. Finishing concrete within a 6 in. x 6 in. x 20 in. beam mold.**

**Table 3. Concrete material properties.**

Test	Design	Truck 1	Truck 2	ASTM Method
Temperature	---	70.1°F	72.5°F	C1064
Air-Content	6.0% ± 1.5%	4.0%	5.4%	C173
Slump	4.0 in. ± 1 in.	5.0 in.	7.25 in.	C143
Unit Weight	145 lb./ft <sup>3</sup>	147 lb./ft <sup>3</sup>	144 lb./ft <sup>3</sup>	C138

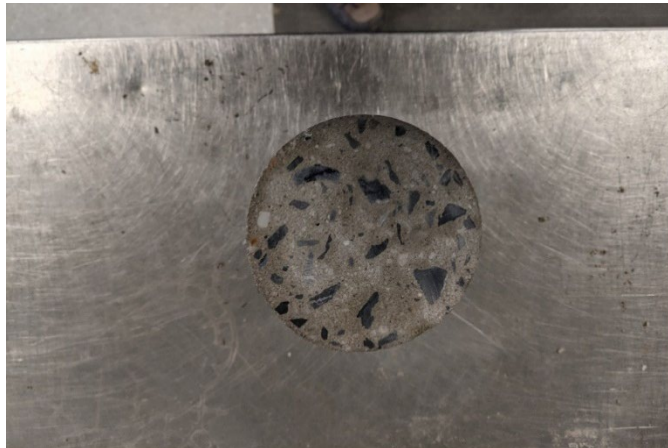
The compressive and flexural tests of the concrete were taken near the time of structural testing of the girders to obtain compressive and tensile strengths of the concrete that are representative of girders at the time of testing. The concrete cylinders were tested at the Concrete Laboratory at the Delaware Department of Transportation (DelDOT).

Prior to the compression tests of the concrete cylinders, the dimensions of the cylinders were measured using calipers. The dimensions of the diameter and length of the cylinders were taken at three separate locations for each cylinder. The average of each dimension was used to determine the compressive strength of the cylinder. The ends of the cylinders were ground at the DelDOT Concrete Laboratory to create flat and level surfaces at the ends of the cylinder (Figure 43 and Figure 44). This ensured that the testing machine evenly applies force to the ends of the cylinder without any stress concentrations. The concrete cylinders were tested following the guidelines stated in ASTM C39. The loading rate for all cylinders remained constant at 35 psi/s. The results from the compressive cylinder tests are shown in

Table 4.



**Figure 43. Grinding the top surface of the concrete cylinder.**

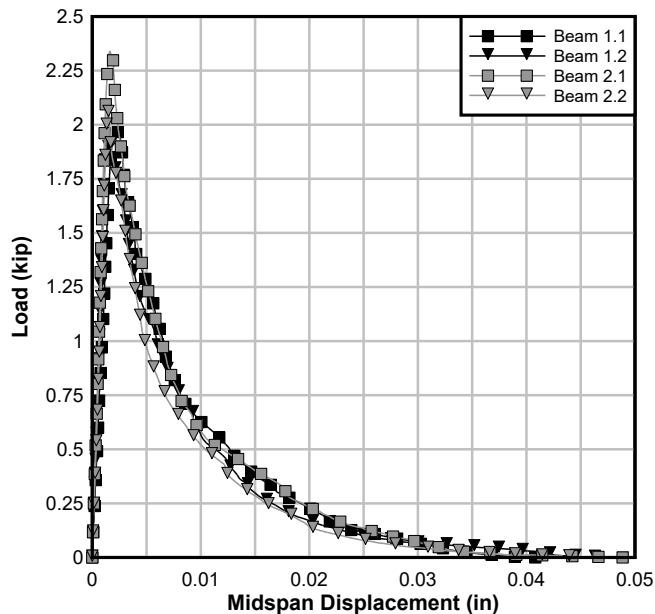


**Figure 44. Typical end result of grinding the top surface of a concrete cylinder.**

**Table 4. Results from compressive cylinder testing at 665 days.**

Truck	Cylinder	Compressive Strength	Average Compressive Strength	COV
		psi	psi	%
Truck 1	1.1	4,740	4,580 ± 151	2.7
	1.2	4,560		
	1.3	4,440		
Truck 2	2.1	4,110	4,290 ± 195	3.5
	2.2	4,270		
	2.3	4,480		

To measure the fracture energy of the concrete, the 6 in. x 6 in. x 20 in. concrete beams were tested on the Instron Machine 1331 load frame with MTS system controls in the Structural Laboratory at the University of Delaware. A total of four concrete beams, two from each truck, were tested under 3-point bending. Prior to the testing, a notch with a 2-in. depth was cut at mid-span of each of the concrete beams for crack propagation. The test was controlled with a constant crack opening rate of 0.015 mm/min after an initial loading of 50 lbf. During the test the crack opening was measured with an extensometer placed at the notch at midspan. The displacements of the concrete beam were measured using two LVDTs at midspan. Figure 45 shows the load versus displacement curves obtained during testing. Table 5 shows the fracture energy and flexural strength results from the testing.



**Figure 45. Load versus displacement curves from fracture energy tests.**

**Table 5. Results from fracture energy tests of concrete at 684 days.**

Truck	Beam	Flexural Strength	Average Flexural Strength	COV	Fracture Energy	Average Fracture Energy	COV
		psi	psi	%	lb/ft	lb/ft	%
Truck 1	1.1	291	329 ± 29	8.9	8.7	10.0 ± 0.9	10.4
	1.2	306			8.7		
Truck 2	2.1	341			10.7		
	2.2	352			8.7		

## REINFORCING STEEL MATERIAL PROPERTIES

Standard Grade 60 reinforcing bars were used as internal steel reinforcement. The tensile properties of the reinforcing bars were tested in the Structures Laboratory at the University of Delaware. The tensile specimens of the reinforcing steel were created by cutting three sections of the longitudinal #6 bars to a 4-ft length (Figure 46). A gauge punch was used to create indents at 2 in. on-center along the length of the tensile specimen to manually calculate elongations.



**Figure 46. Typical 4-ft section of #6 rebar used for tensile tests.**

A 3D digital image correlation system was used to measure the strain in the rebar during loading. The DIC system consisted of two cameras with 50-mm lenses placed on an adjustable bar at 27 in. apart from one another. The DIC system was tilted 90 degrees to better capture the field of view of the rebar tensile test, as the field of view of the system has a greater width compared to its height. The DIC system actively recorded the displacement at given points during the loading of the tensile specimen. To capture the displacements of the rebar during the loading, a contrasting speckled pattern had to be applied to the bar. The mill scale was first ground off of the rebar using a wire-wheel brush to ensure that the speckled pattern would not flake off during its elongation. A coat of flat-white spray paint was applied to the rebar followed

by flat-black spray paint to create a contrasting speckled pattern at about a 50-50 coverage rate. The DIC system is then able to create a finite element mesh on the surface of the rebar using the speckled pattern as a reference. The DIC system was then able to calculate the displacements and strains over the entire surface of the rebar during its loading.

The tensile tests of the #6 reinforcing bars were completed on a Tinius Olsen 200k Super L Universal Testing Machine per the guidelines stated in ASTM A370 and ASTM A615. The tensile specimens were loaded at a rate of 50,000 psi/min per ASTM A370 until rupture of the steel (Figure 47). The stress-strain curves obtained during the testing can be seen in Figure 48. The stress-strain curves were determined from the data obtained from both the Tinius Olsen and the DIC system. The loads were obtained from the Tinius Olsen and outputted to the DIC system, which calculated the strain. Table 6 shows the material properties of the rebar obtained from the tensile testing. The material properties of the rebar were calculated per the methods presented in ASTM A370.



**Figure 47. Ruptured rebar tensile test specimen.**

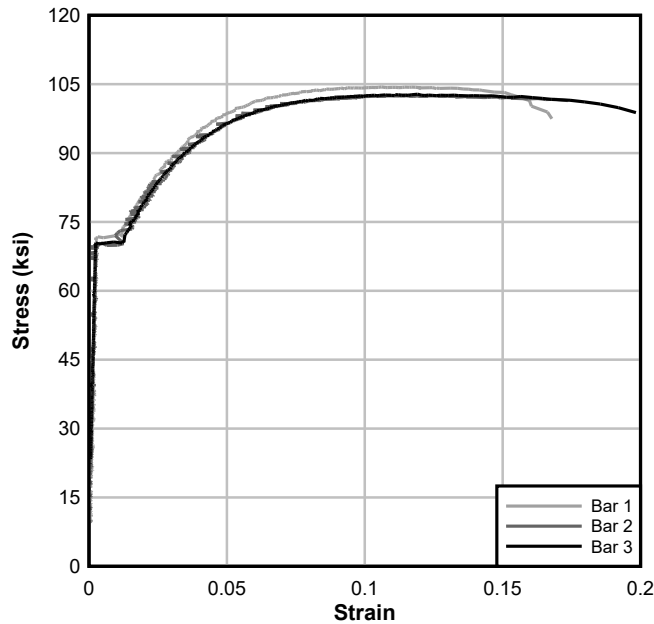


Figure 48. Stress strain curves of #6 rebar tensile test specimens.

Table 6. Results of #6 rebar tensile tests.

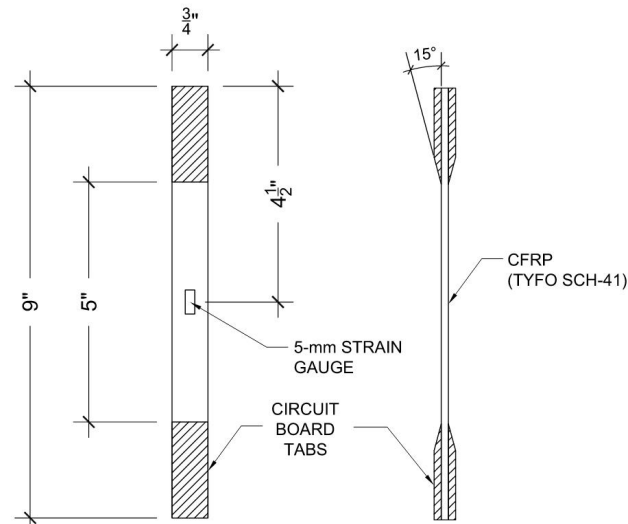
Bar	Elastic Modulus	Yield Stress	Strain at Yield	Strain at Strain Hardening	Ultimate Stress	Strain at Ultimate	Strain at Rupture
	ksi	ksi	%	%	ksi	%	%
Bar 1	29,100	71.1	0.245	1.14	104	10.6	16.8
Bar 2	26,400	69.1	0.262	1.03	102	11.5	17.3
Bar 3	29,200	70.0	0.240	1.26	103	11.9	19.8
Average ± STD	28,200 ± 1590	70.0 ± 1.0	0.249 ± 0.01	1.14 ± 0.1	103 ± 1	11.3 ± 0.6	18.0 ± 1.6
COV	5.6%	1.4%	4.6%	10.1%	1.0%	5.9%	9%

## CARBON FIBER REINFORCED POLYMERS MATERIAL PROPERTIES

Fyfe Tyfo SCH-41 CFRP composite was used to strengthen the reinforced concrete girders. The CFRP consists of unidirectional carbon fiber fabric and a two-part epoxy (Tyfo S Epoxy). The manufacturer’s properties of the CFRP state a tensile strength in the primary direction of the fibers of 143 ksi, an elastic modulus of 13,900 ksi, and a maximum elongation of 1.0%.

A total of six witness panels, measuring 12 in. x 12 in., were fabricated each time CFRP was installed on a reinforced concrete girder following the guidelines stated in ASTM D3039. Table 9 in the appendix outlines the process for the creation of witness panels. After a 7-day curing period, the witness panels were cut into 9 in. by 0.75 in. tensile coupons using a wet-tile saw. The grips for the tensile coupons were made from a composite circuit board, which was recommended by the material manufacturer. The circuit board was cut to the dimensions of the grips given in ASTM D3039. The edges of the grips were sanded to create a 10-

to 15-degree taper to avoid stress concentrations at the edges of the grips. Both the surfaces of the tabs and tensile coupons were lightly sanded to provide a rough surface to bond to the two materials. The materials were bonded using a two-part epoxy that was recommended by the manufacturer, Loctite E-20hp. The thickness of the bond line between the tab and the CFRP coupon was controlled using a metal wire to create a bond thickness of 0.02 inches. Figure 49 shows a drawing of a typical CFRP coupon.



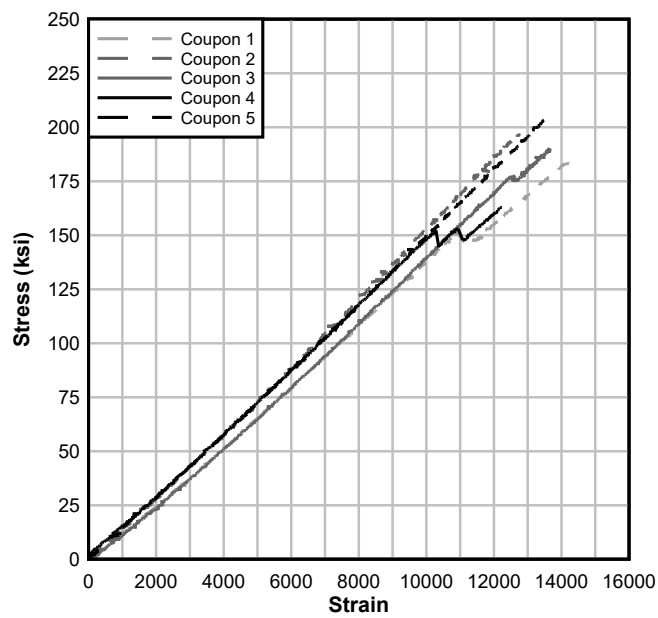
**Figure 49. Drawing of CFRP tensile coupons.**

Five tensile coupons were tested on an Instron Machine 1331 load frame with MTS system controls in the Structural Laboratory at the University of Delaware. The tensile coupons were instrumented with 5-mm strain gauges on one side of the coupon. The DIC system was incorporated into the CFRP tensile coupon testing, similar to the rebar tensile test. To account for the DIC system, a contrasting speckled pattern had to be applied to the other face of the tensile coupon so that strains could be calculated during its loading. Each of the tensile specimens was loaded in a displacement-controlled test at a constant rate of 0.01 in/min until the specimens reached rupture (Figure 50). The material properties of the CFRP gathered from the testing of the tensile coupons are shown in Table 7. Figure 51 shows the tensile stress-strain curves obtained during the material testing.





**Figure 50. Typical failure mode observed during CFRP tensile testing.**



**Figure 51. Results from the CFRP tensile coupon tests.**

**Table 7. CFRP tensile coupon test results.**

<b>CFRP Coupon</b>	<b>Tensile Strength</b>	<b>Maximum Strain</b>	<b>Elastic Modulus</b>
	<b>ksi</b>	<b>10<sup>-6</sup> in./in.</b>	<b>ksi</b>
Coupon 1	184	14,200	13,700
Coupon 2	197	12,700	15,300
Coupon 3	190	13,600	13,800
Coupon 4	163	12,200	14,700
Coupon 5	204	13,600	14,800
Average ± STD	181 ± 16	13,200 ± 700	14,400 ± 540
COV	8.8%	5.3%	3.8%

## CHAPTER 6

# Results and Discussion

### FLEXURAL BEHAVIOR

The total load versus displacement plots and results from the 12 girders tested can be seen in Figure 52 and Table 8. Each of the girders exhibited tri-linear behavior with defined stages corresponding to uncracked concrete, cracked concrete, and the yield of the tensile reinforcing steel. The unstrengthened control girder, 0L0U, experienced a tension-controlled flexural failure with an ultimate load capacity of 44.2 kips. The addition of longitudinal CFRP (without anchorage) to the girder resulted in increases of 28%, 64%, and 98% for one, two, and three plies of CFRP, respectively, when compared to 0L0U. However, this also resulted in a notable decrease in ductility.

Further increases in flexural capacity were observed when U-Wrap anchors were applied to the flexural CFRP. Increases of ultimate capacity of 14% and 20% were observed for 1L1U-8 and 1L2U-16, respectively, when compared to 1L0U. It should be noted that 1L2U-16 exhibited a greater flexural capacity as well as ductility compared to 1L1U-8. Both of the girders had the same  $A_{prov}$  and the same cross-sectional area of the longitudinal CFRP. 1L2U-16 had U-Wraps at a larger spacing, which may have increased the flexural capacity and ductility of the girder.

The specimens with 2 plies in the longitudinal CFRP exhibited similar flexural behavior among each other (Figure 52). 2L1U-8 exhibited the least improvement in ultimate load capacity at an increase of 22% compared to 2L0U. 2L2U-8 and 2L3U-8 exhibited similar increases in load capacity of 24% and 25%, respectively, compared to 2L0U. Likewise, the girders with 3 plies in the longitudinal CFRP also exhibited comparable flexural behavior among the three of them (3L1U-8, 3L2U-8, and 3L3U-8) (Figure 52). Increases in ultimate capacity ranging from 14% to 21% were observed compared to 3L0U. It should be noted that 3L1U-8 exhibited the least improvement in ultimate capacity at 14%. Ultimately, the number of plies within the U-Wrap anchors did not have a notable effect on increasing the load capacity of a girder.

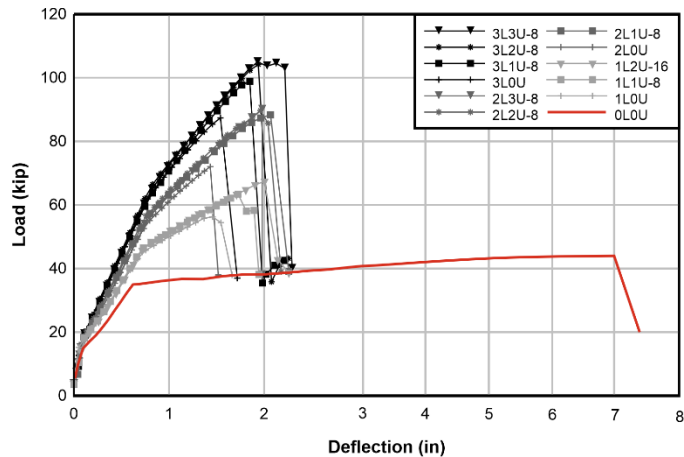


Figure 52. Load versus midspan deflection plots of all 12 girders tested.

Table 8. Summary of Test Results.

Girder	$P_{cr}$	$P_y$	$P_u$	$\Delta_u/\Delta_y$	Maximum Strain of CFRP	Failure Mode
	kip	kip	kip		$10^{-6}$ in/in	
0L0U	12.7	35.2	44.2	9.43	N/A	Tension-controlled flexural
1L0U	17.1	45.8	56.6	1.88	8090	IC Debonding
1L1U-8	17.1	46.5	64.5	2.46	12400	Longitudinal CFRP Rupture
1L2U-16	17.3	47.4	68.0	2.66	12700	Longitudinal CFRP Rupture
2L0U	16.0	54.2	72.4	1.91	6870	IC Debonding
2L1U-8	18.6	57.6	88.6	2.49	9960	U-Wrap Rupture
2L2U-8	18.2	57.6	89.7	2.45	9750	Complete U-Wrap Debonding
2L3U-8	16.9	57.1	90.7	2.44	10100	Partial U-Wrap Debonding or U-Wrap Interface Failure*
3L0U	17.7	61.8	87.5	1.99	6630	IC Debonding
3L1U-8	17.5	64.0	99.3	2.24	9900	U-Wrap Rupture
3L2U-8	17.3	65.4	104	2.40	9250	Complete U-Wrap Debonding
3L3U-8	18.5	63.8	106	2.48	9730	Concrete Crushing

$P_{cr}$ : Load at cracking of concrete in tension

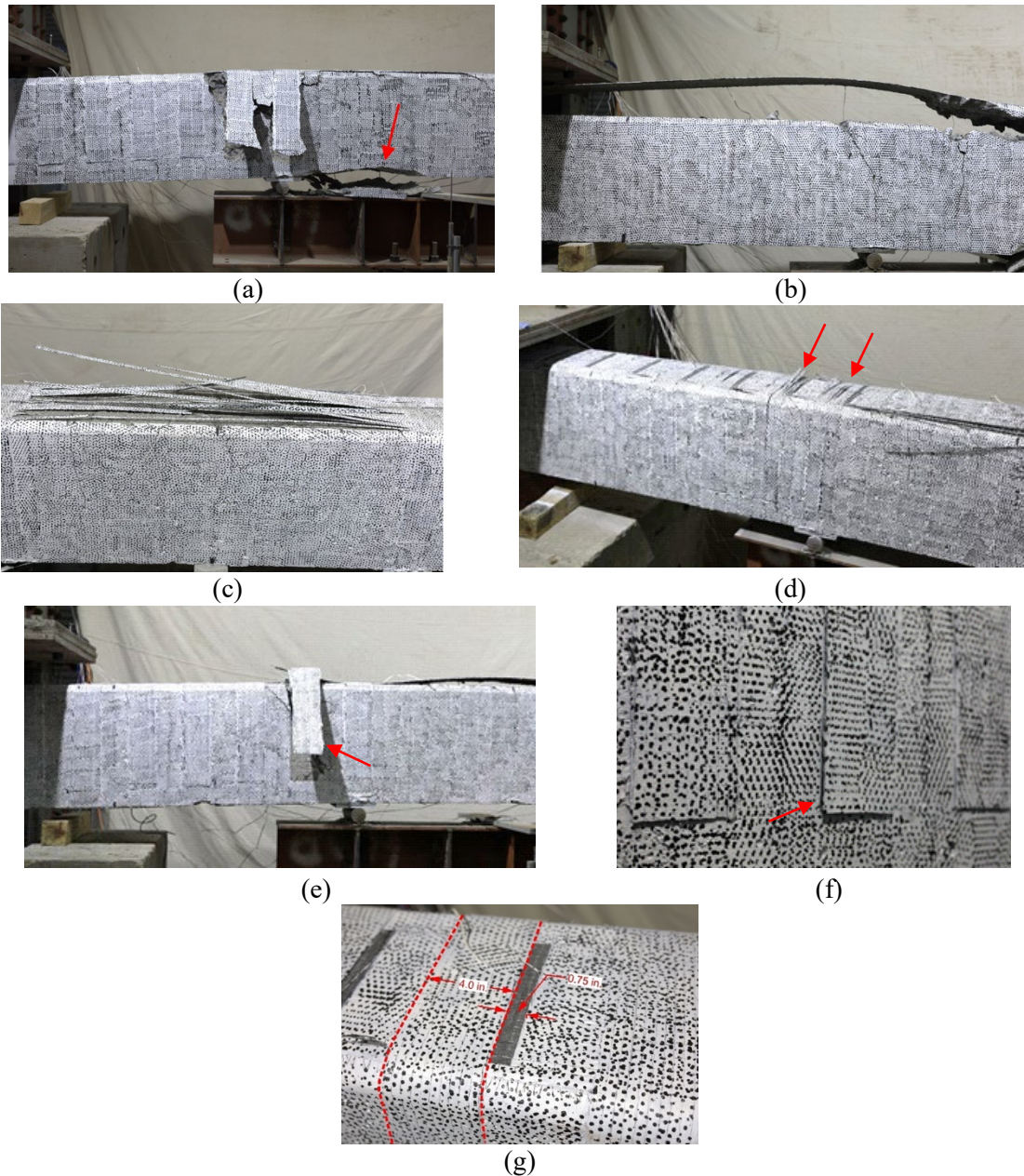
$P_y$ : Load at yield of the steel reinforcement

$P_u$ : Load at ultimate capacity

$\Delta_u/\Delta_y$ : ratio of the displace at ultimate load ( $\Delta_u$ ) to displacement at steel yielding ( $\Delta_y$ )

\* Unclear whether the primary failure mode was partial U-Wrap debonding or U-Wrap interface failure

The failure modes that were observed during the experimental testing of CFRP-strengthened beams were concrete crushing, rupture of the longitudinal CFRP, partial debonding of the U-Wrap anchors, complete debonding of the U-Wrap anchors, adhesive failure at the interface between the U-Wrap and longitudinal CFRP (herein referred to as U-Wrap interface failure), and rupture of the U-Wrap anchors. The representative examples of failure modes of the girders can be seen in Figure 53, and photographs of the failure modes for the remaining girders can be found in the appendix.



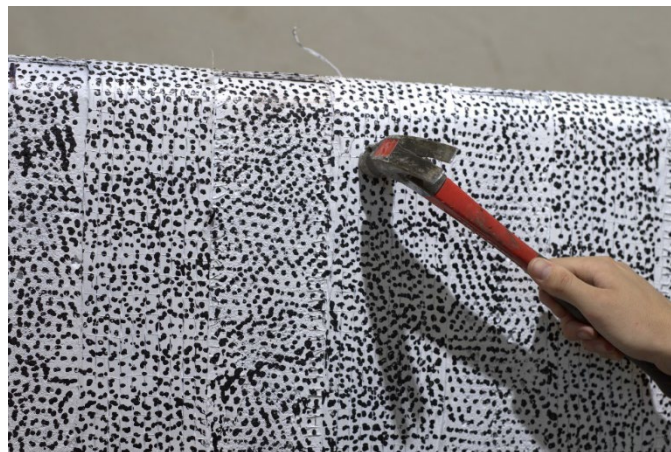
**Figure 53. Typical failure modes in CFRP-strengthened beams: (a) concrete crushing (3L3U-8) (arrow points to the primary failure mode of concrete crushing); (b) IC debonding (2L0U); (c) longitudinal CFRP rupture (1L1U-8); (d) U-Wrap anchor rupture (arrows point to ruptured anchors on girder 2L1U-8); (e) complete debonding of U-Wrap anchor (arrow points to debonded anchors on girder 2L2U-8); (f) partial debonding of U-Wrap anchor (arrow points to partially debonded anchor on girder 2L3U-8); (g) U-Wrap interface failure in Girder 2L2U-8 (dashed lines outline the U-Wrap anchor).**

The strengthened control girders, 1L0U, 2L0U, and 3L0U, each failed by IC debonding (Figure 53b). U-Wraps delayed IC debonding in all the anchored girders and even led to the rupture of the laminate in 1L1U-8 and 1L2U-16. The rupture of the laminate occurred within the constant moment region for each of these girders (Figure 53c). 1L1U-8 and 1L2U-16 developed higher strains in the longitudinal CFRP compared to the other anchored specimens, as there was only one ply of CFRP in the laminate. The debonding strain of

flexural CFRP is inversely proportional to the number of plies of CFRP in the laminate (ACI Committee 440, 2017). Thus, since 1L1U-8 and 1L2U-16 only had one ply of longitudinal CFRP, higher strains were developed compared to the other anchored specimens, allowing the 1L specimens to reach the rupture strain of the longitudinal CFRP.

The remaining girders had either 2 or 3 plies in the longitudinal CFRP and 1, 2, or 3 plies of CFRP in the U-Wraps. The spacing of the U-Wrap anchors remained constant at 8 in. on-center within the shear spans. Each of the girders with one ply in the U-Wraps, 2L1U-8 and 3L1U-8, failed by rupture of the U-Wrap anchors (Figure 53d). U-Wraps 7 and 8 ruptured in 2L1U-8 and U-Wraps 1 through 8 ruptured in 3L1U-8. U-Wrap 7 on 3L1U-8 also exhibited debonding from the concrete substrate. Both 2L1U-8 and 3L1U-8 recorded the lowest increase in strength (22% and 14%, respectively) compared to the other anchored specimens with 2 and 3 plies of longitudinal CFRP. The strength gain in both girders was limited due to the rupture of the U-Wraps. When the thickness of the U-Wraps was increased to 2 or 3 plies, failure modes such as U-Wrap debonding and U-Wrap interface failure were observed. Increasing the thickness of the U-Wraps was shown to mitigate U-Wrap rupture.

The girders 2L2U-8, 2L3U-8, and 3L2U-8 each failed by U-Wrap debonding. Both complete and partial U-Wrap debonding were observed among these specimens (Figure 53e and Figure 53f, respectively). Complete U-Wrap debonding occurred when the U-Wrap abruptly delaminated from the concrete substrate while also removing concrete cover. Complete U-Wrap debonding was visibly apparent during the post-mortem inspections of the girders (Figure 55). The U-Wraps were determined to be partially debonded by gently tapping on the U-Wraps with a hammer to find hollow areas where the CFRP had delaminated from the concrete substrate (Figure 54).



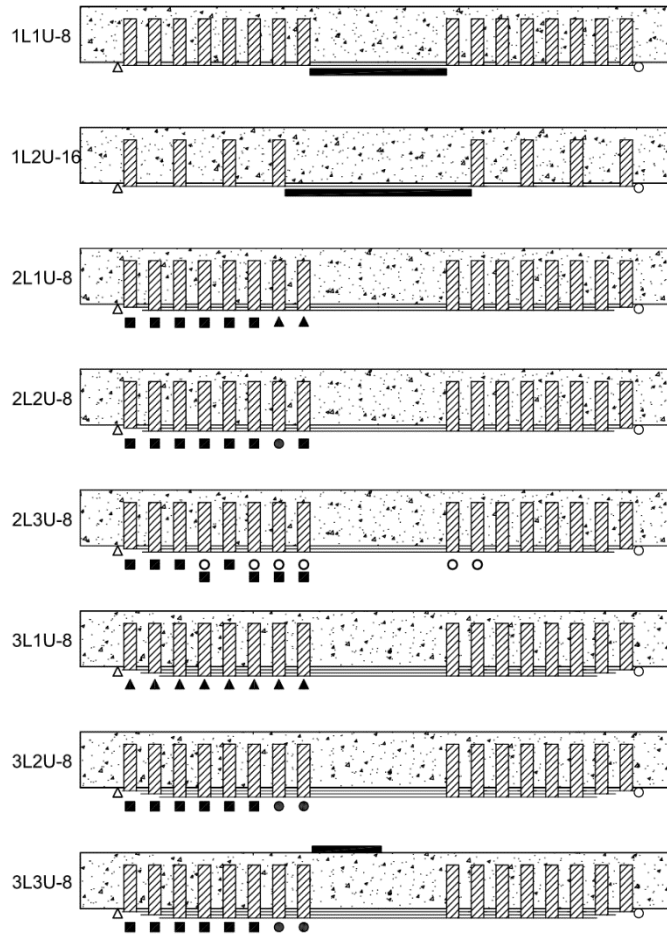
**Figure 54. Sounding the U-Wraps to determine whether the U-Wraps are partially debonded.**

2L3U-8 showed isolated partial debonding of the U-Wraps throughout its shear spans (Figure 53f). 2L3U-8 also exhibited U-Wrap interface failure at U-Wraps 1 through 8. While U-Wrap interface failure was evident, it is unclear whether the failure occurred before or after the partial debonding of the U-Wrap anchors. This was due to the abrupt, brittle failure of CFRP and the slow acquisition rate of the DIC system. Therefore, the primary failure mode of 2L3U-8 was determined to be due to a combination of partial U-Wrap debonding and U-Wrap interface failure (Figure 53f and Figure 53g, respectively).

U-Wrap 7 completely debonded from the concrete substrate on 2L2U-8 and removed a large amount of concrete cover (Figure 53e). 3L2U-8 failed once U-Wraps 7 and 8 completely debonded from the concrete substrate. 3L3U-8 was the only strengthened girder to fail by concrete crushing. 3L3U-8 initially failed by concrete crushing at a maximum load of 105.8 kip followed by an immediate drop in load and some residual strength until U-Wraps 7 and 8 debonded. When 3 plies were added to the U-Wraps, increases in strength of 1% (2L3U-8) and 2% (3L3U-8) were observed when compared to the specimens with 2 plies in the U-Wraps (2L2U-8 and 3L2U-8, respectively). The experimental data from this study shows that increasing the thickness of the U-Wrap anchors by adding successive plies of CFRP to the anchors does not result in a notable increase in load capacity, specifically after U-Wrap rupture was mitigated. After U-Wrap rupture is mitigated, the effectiveness of the U-Wraps may be dependent on the adhesive bond between the longitudinal CFRP and the U-Wraps, as U-Wrap interface failure was observed in each of the girders (Figure 55).

U-Wrap interface failure indicates a failure of the adhesive bond between the first ply of the U-Wraps and the longitudinal CFRP (Figure 53g). U-Wrap interface failure was only determined to be a primary failure mode of 2L3U-8, since the U-Wraps that were partially debonded also exhibited U-Wrap interface failure. U-Wrap interface failure was not observed on the U-Wraps that completely debonded or ruptured. However, the remaining U-Wraps that did not rupture or completely debond on the girder all exhibited U-Wrap interface failure. Figure 55 shows post-mortem inspections of the girder, where the failure modes and U-Wrap interface failure are both displayed.





**Figure 55. Post-mortem inspection of girders with U-Wrap anchorage (● complete U-Wrap debonding, ○ partial U-Wrap debonding, ▲ U-Wrap Rupture, — longitudinal CFRP rupture or concrete crushing, ■ U-Wrap interface failure).**

The addition of longitudinal CFRP to the girders increased the maximum load; however, it came at the expense of a decrease in ductility. To determine the ductility, the yield of the tensile steel reinforcement was defined as the point where the load versus deflection curve underwent a sudden decrease in slope for the second time. Ductility coefficient ( $\mu$ ) is defined as the midspan deflection at ultimate load ( $\Delta_u$ ) divided by the midspan deflection at the yield of the tensile steel reinforcement ( $\Delta_y$ ) (Equation 5).

$$\mu = \frac{\Delta_u}{\Delta_y}$$

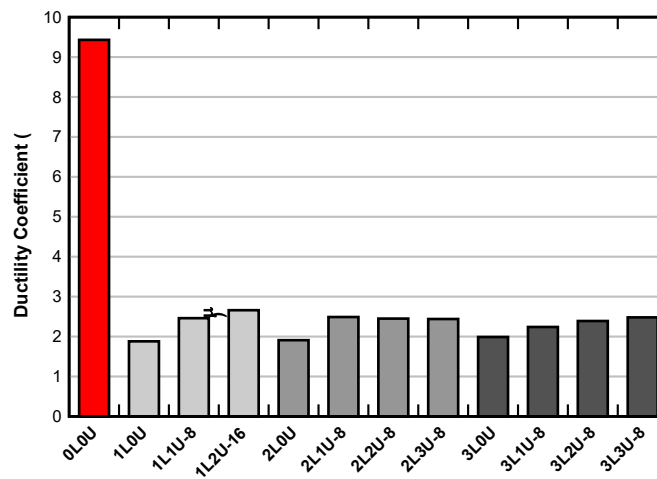
5

The addition of CFRP to the concrete girder resulted in a decrease in ductility as much as 80% (1L0U) (Figure 56). However, the addition of U-Wrap anchors to the longitudinal CFRP increased the ductility of each girder when compared to their respective unanchored control girder. U-Wraps increased the ductility

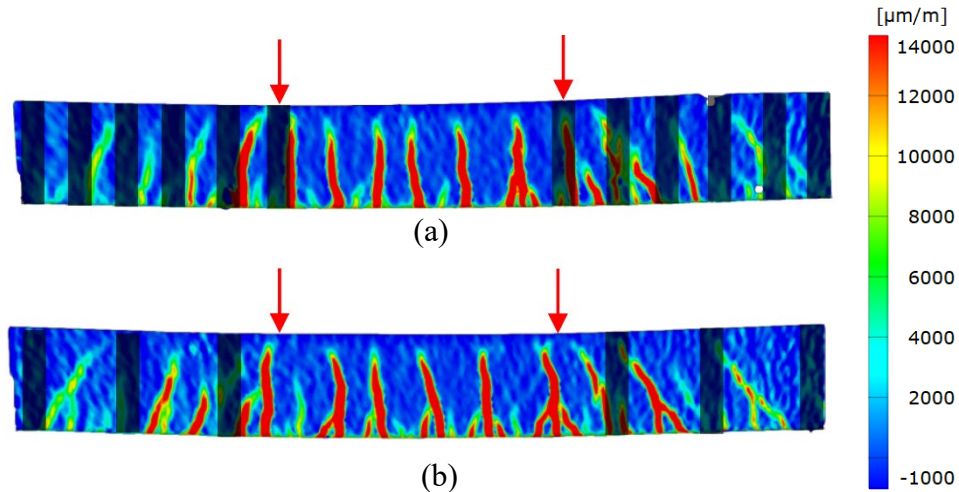
of a strengthened girder by 27% on average. It should be noted that there was a similar ductility among most of the girders with U-Wraps spaced at 8 in. on-center. The similar ductility among the girders with U-Wraps spaced at 8 in. on-center can be attributed to flexural cracks being contained between the U-Wrap anchors. This led to similar crack patterns of the girders with U-Wraps spaced at 8 in. on-center. Figure 57a shows the flexural cracks at ultimate load observed by the DIC system. The cracks are indicated as areas of high strain (red).

Interestingly, there was a 9% increase in ductility in girder 1L2U-16 compared to 1L1U-8. It should be noted that each girder also had the same  $A_{prov}$ ; however, 1L2U-16 had a greater spacing of the U-Wraps within the shear spans at 16 in. on-center. While statistical significance is lacking, one possible explanation for the increased ductility of 1L2U-16 is the greater spacing of the U-Wrap anchors within the shear spans. As previously stated, the flexural cracks were primarily contained between the U-Wraps. Since the U-Wraps had a greater spacing in 1L2U-16, the flexural cracks had more room to propagate compared to the 1L1U-8.

Figure 57b shows the crack pattern at flexural capacity for 1L2U-16. The crack patterns of the remaining girders are shown in Figure 81 through Figure 84 in the appendix.



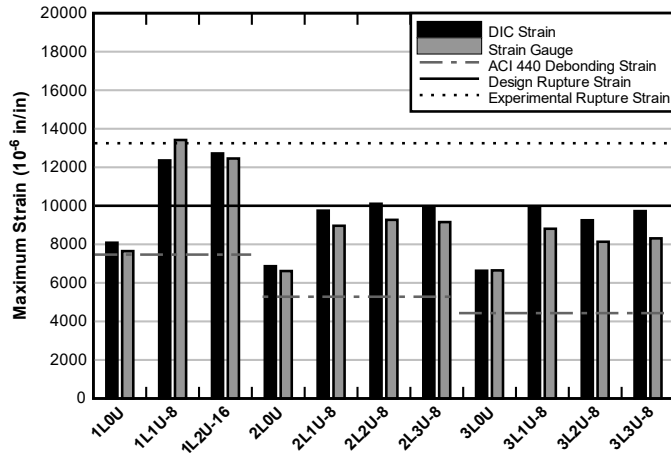
**Figure 56. Summary of ductility coefficients of all 12 girders.**



**Figure 57. Typical crack patterns at failure (arrows represent the approximate locations of the loading points on the girder and shaded bars represent the approximate locations of the U-Wraps): (a) Girder 1L1U-8; (b) Girder 1L2U-16.**

## STRAIN IN LONGITUDINAL CFRP

The DIC system captured the strain of the longitudinal CFRP during the four-point bending of the girders. The maximum strain of the longitudinal CFRP was captured within the middle third of the CFRP within the constant moment region. The surface created by the DIC system was modified to remove the locations where strain gauges were placed on the CFRP, as the strain gauge wires resulted in noise in the data. The maximum strain obtained from the DIC system was then compared to the maximum strain recorded by the strain gauges. Figure 58 shows the maximum strain in the longitudinal CFRP at ultimate load compared to the maximum strain obtained by the strain gauges. Additionally, the estimated debonding strains of the longitudinal CFRP according to ACI 440 Committee 440 (2017), the rupture strain given by the material manufacturer, and the rupture strain obtained from the material testing are shown for reference.



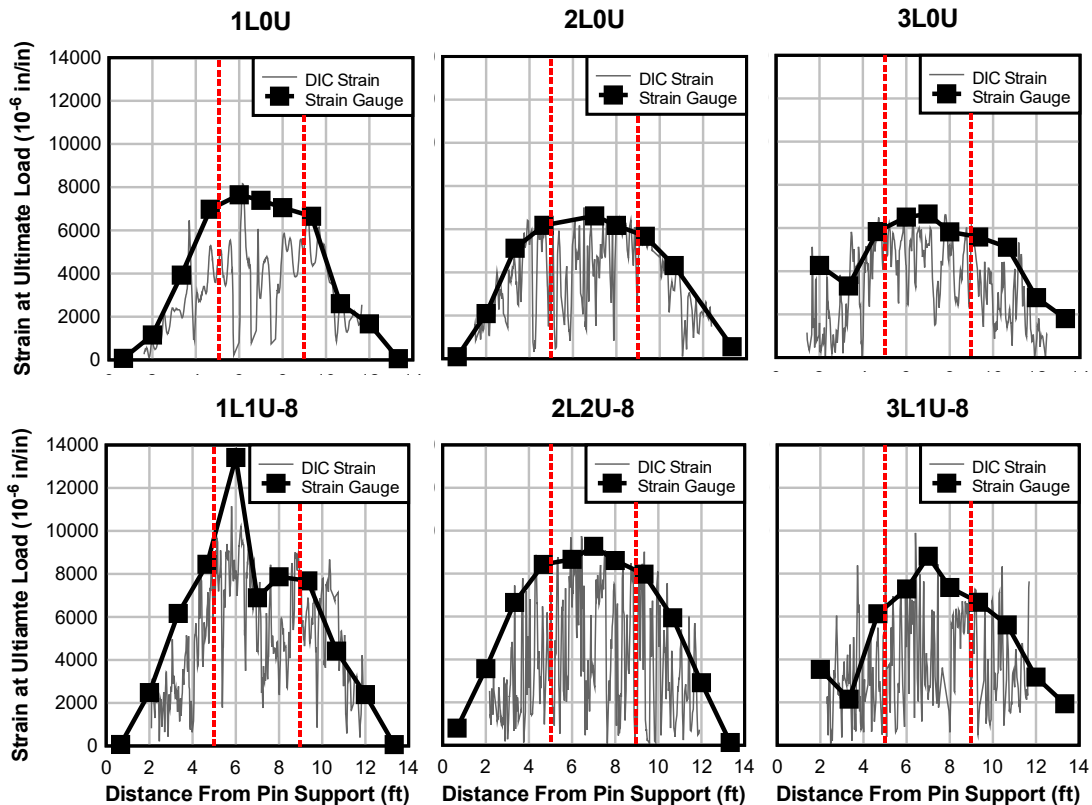
**Figure 58. Summary of maximum strains of the longitudinal CFRP.**

On average, the maximum strain recorded by the DIC system exceeded the maximum strain obtained from the strain gauges (Figure 58). This was to be expected, as the DIC system was capturing strain throughout the entire constant moment region, whereas the strain gauges were recording strain at three fixed points within the constant moment region.

Figure 59 shows a plot comparing the strains at ultimate load recorded by the strain gauges and the DIC system for the three strengthened control girders as well as three girders representative of the anchored girders. The strains in

Figure 59 were computed from a representative section (line) along the length of the girder with evenly distributed data points to show the peaks and valleys of strains recorded in the longitudinal CFRP. The strain values observed in

Figure 59 do not correspond to the maximum observed strains of the longitudinal CFRP as observed in Figure 58. The peaks in the longitudinal CFRP strain occurred at locations where the concrete cracked in tension. The CFRP bridged the cracks in the concrete, which resulted in a sharp increase in strain in the CFRP at the locations of the flexural cracks. The DIC system was able to capture the peaks in strain of the longitudinal CFRP more closely than the strain gauges, since the DIC system captured strains along the entire length of the girder.



**Figure 59. Comparison of strains along the length of the unanchored control girders at flexural capacity (vertical dashed lines show the limits of the constant moment region).**

The unanchored control girders each exceeded the debonding strain of the longitudinal CFRP calculated according to ACI Committee 440 (2017). The measured maximum strains of the longitudinal CFRP were 8%, 30%, and 50% greater than the calculated debonding strain for 1L0U, 2L0U, and 3L0U, respectively. The addition of U-Wraps to the longitudinal CFRP allowed the girders to exceed the maximum strain of their corresponding unanchored control girders. Each of the anchored specimens in the 1L group exceeded the rupture strain given by the material manufacturer. Increases in strain as much as 57% (1L2U-16) were observed compared to 1L0U. The addition of U-Wraps to the girders with 2 and 3 plies of longitudinal CFRP resulted in a consistent increase in strain of longitudinal CFRP. Increases in strain of 40% to 49% were observed compared to their respective unanchored control girders with 2 and 3 plies of longitudinal CFRP. The consistency of the increases in strain among these specimens can be attributed to the failure modes. Each of the girders with 2 and 3 plies of longitudinal CFRP exhibited failure of the U-Wraps, whether it was rupture, debonding, or U-Wrap interface failure.

The DIC system was also utilized to capture strains in U-Wraps. U-Wraps 1, 2, 15, and 16 were not within the field of view of the DIC system. The maximum strain of each of the U-Wraps was taken at the ultimate load of the girder (Figure 60). The maximum, minimum, and median strains of the U-Wraps were recorded and plotted against each of the girders for comparison (Figure 61). Like flexural CFRP, U-Wraps have an effective strain estimated by ACI Committee 440 (2017) for shear design. As shown in Figure 61, the U-Wraps in all girders exceeded the effective strain given by ACI Committee 440 (2017) except for one U-Wrap in 3L1U-8. There is no apparent trend of the observed strains in the U-Wraps among the experimental

data. Increasing the number of plies in the U-Wraps appeared to have no effect on the recorded strain in the U-Wraps. The strain developed in the U-Wraps may not be dependent on the number of plies in the U-Wrap.

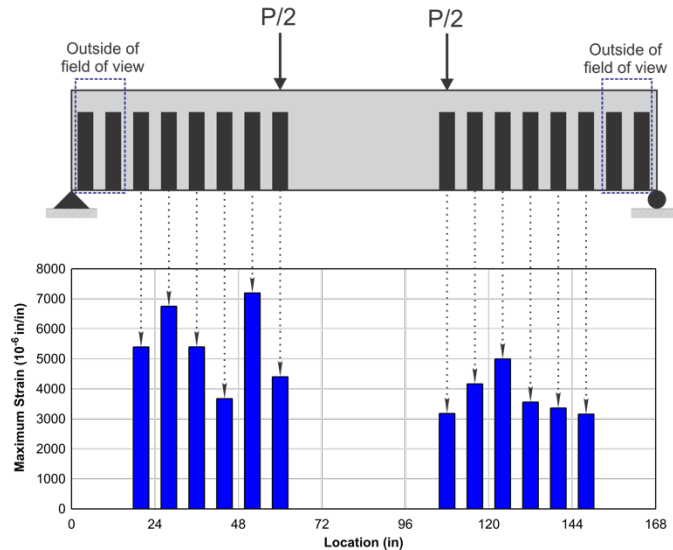


Figure 60. Example peak U-Wrap strain data from girder 2L2U-8.

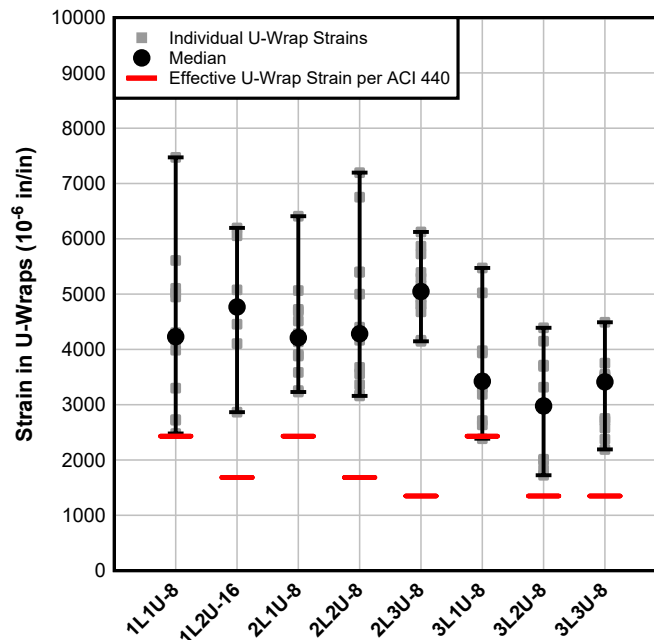


Figure 61. Summary of peak U-Wrap strains observed in the anchored girders (range bars indicate the maximum and minimum observed strains in the U-Wraps).

## COMPARISON TO MODELS

Analytical models of each of the girders were developed in Response-2000 (Bentz, 2000). The material properties of the concrete and steel that were obtained from materials characterization experiments were used in the models. The concrete and steel material properties remained constant between the models. CFRP was modeled as a linear elastic material with an elastic modulus of 13,900 ksi. The maximum strain in longitudinal CFRP was specified based on the measured strain in the longitudinal CFRP at flexural capacity, recorded by the DIC system. The failure of the models typically occurred when the longitudinal CFRP reached its maximum strain, except for 3L1U-8 and 3L3U-8, which both failed by concrete crushing due to the large increase in strength from three plies of longitudinal CFRP. This was generally consistent with our experimental observations, as compressive cracks were observed in 2 of the 3 girders with 3 plies in longitudinal CFRP (3L2U-8 and 3L3U-8). However, 3L3U-8 was the only girder to fail by concrete crushing. The models that failed at the maximum stress of the CFRP were also consistent with the experimental observations, as failure was defined with the recorded maximum strain in the experiment and a linear elastic model was assumed. It should be noted that a majority of the anchored girders within the experimental data failed by U-Wrap rupture, U-Wrap debonding, or U-Wrap interface failure. U-Wrap anchors could not be explicitly modelled in Response-2000; therefore, the models relied on the material

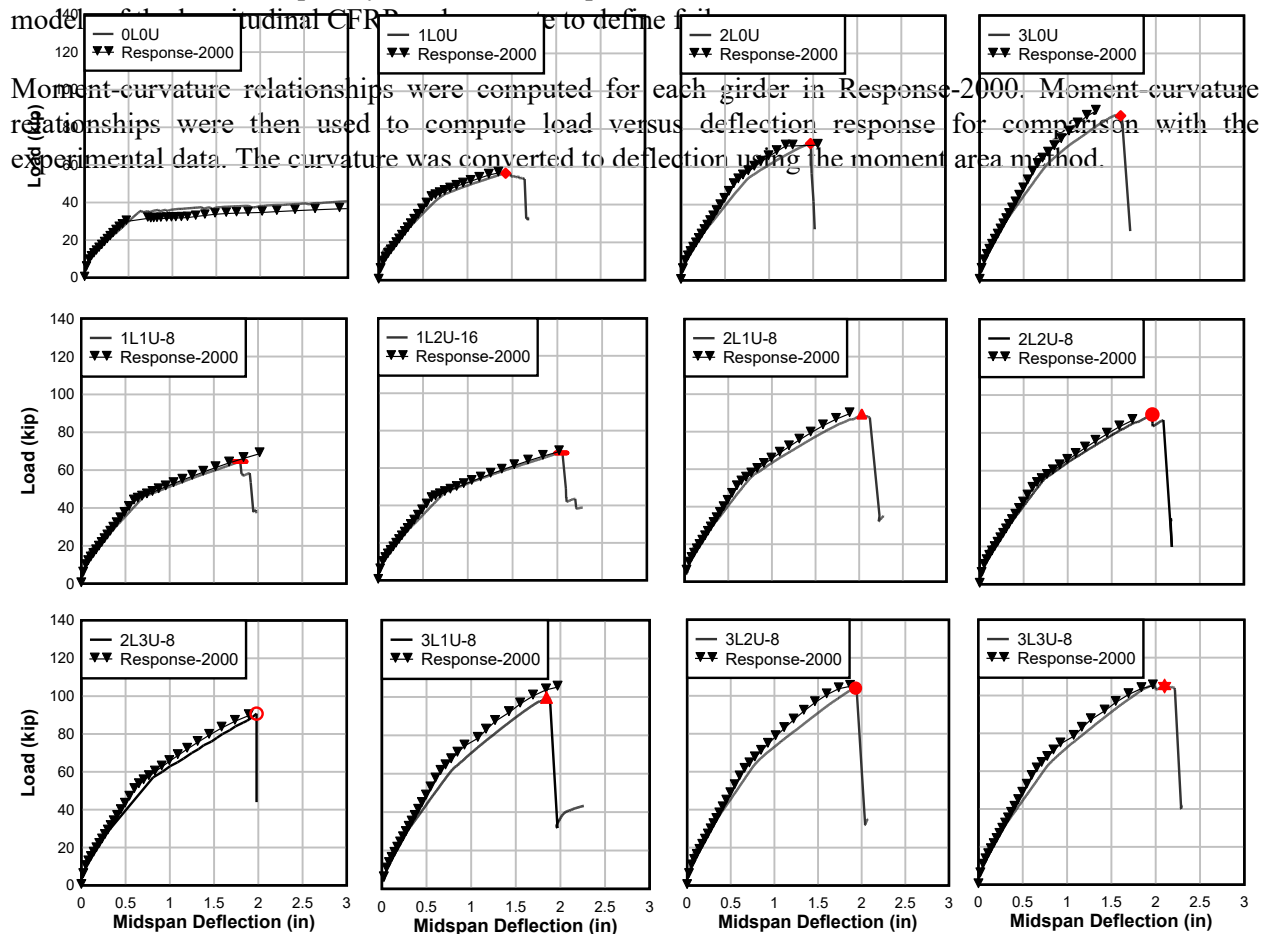


Figure 62 shows the comparison of load versus deflection between the experimental data and the analytical models. The flexural behavior of the Response-2000 models closely resembles the observed flexural behavior in the experimental testing. The ultimate load capacity of the Response-2000 model was between 1% and 13% error of the ultimate load capacity of the experimental data. The load at yield of the tensile

steel reinforcement was between 5 and 13% error of the load observed in the experimental data. The ductility of the models showed the greatest error when compared to the experimental data, which was between 1% and 34% error. From the comparison to the experimental data, there is a high confidence in the ability of the Response-2000 models to accurately predict the flexural behavior and ultimate load capacity of girders strengthened with CFRP. However, the Response-2000 model should not be used to predict the failure modes of strengthened girders, as U-Wraps cannot be explicitly implemented in the models.

The analytical models were used to examine the strain in the longitudinal steel reinforcement and curvature in each of the strengthened girders at flexural capacity. Curvature is representative of the combined strain of the tensile steel reinforcement ( $\epsilon_t$ ) and concrete at the extreme compression fiber ( $\epsilon_{cu}$ ) at flexural capacity. When the curvature exceeds a value of 0.008, the member is classified as a tension-controlled member according to ACI Committee 318 (2019).

The longitudinal steel reinforcement in the strengthened control girders (1L0U, 2L0U, and 3L0U) each reached a strain greater than 0.005 (Figure 63). However, 1L0U was the only strengthened control girder to be classified as a tension-controlled member. All the remaining girders anchored with U-Wraps exceeded the curvature of 0.008 at the tension-controlled limit. In reinforced concrete flexural design, it is more desirable to have tension-controlled members to ensure adequate life safety (ACI Committee 318, 2019). When a section is tension-controlled, higher strength reduction factors can be used to account for the ductile failure mode of the section. Additionally, the higher strength reduction factor typically allows for a more cost-effective (less conservative) design. The addition of U-Wraps to the girders with 2 and 3 plies in the longitudinal CFRP allowed the girders to exceed the curvature at the tension-controlled limit, while their respective unanchored control girders did not.



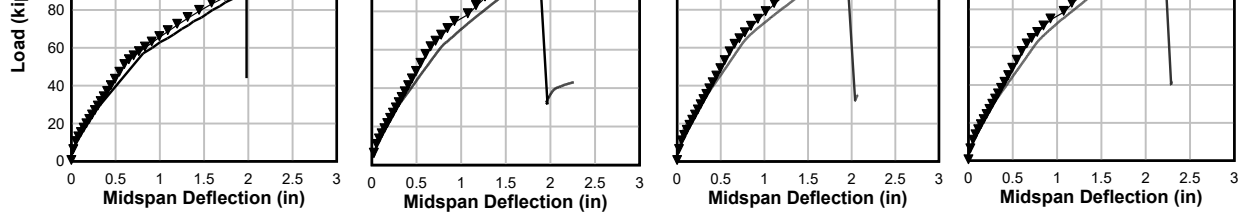


Figure 62. Comparison of the experimental data to the Response-2000 model (◆ IC debonding, — longitudinal CFRP rupture, ● complete U-Wrap debonding, ○ partial U-Wrap debonding and U-Wrap interface failure, ▲ U-Wrap Rupture, ★ concrete crushing).

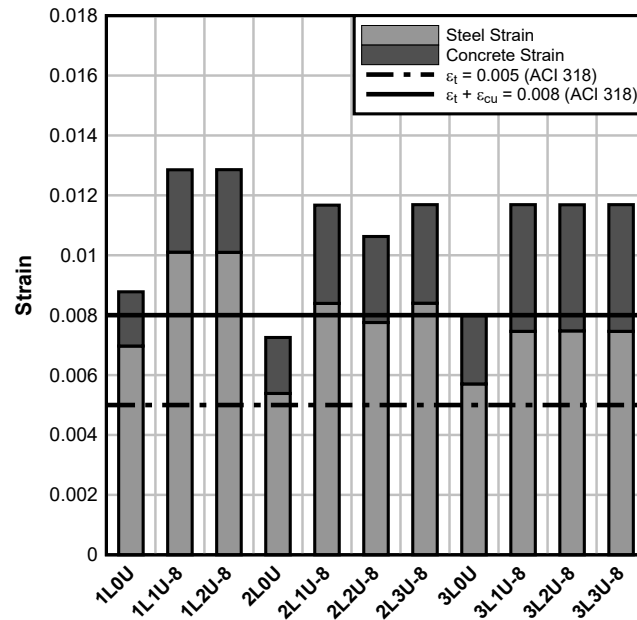


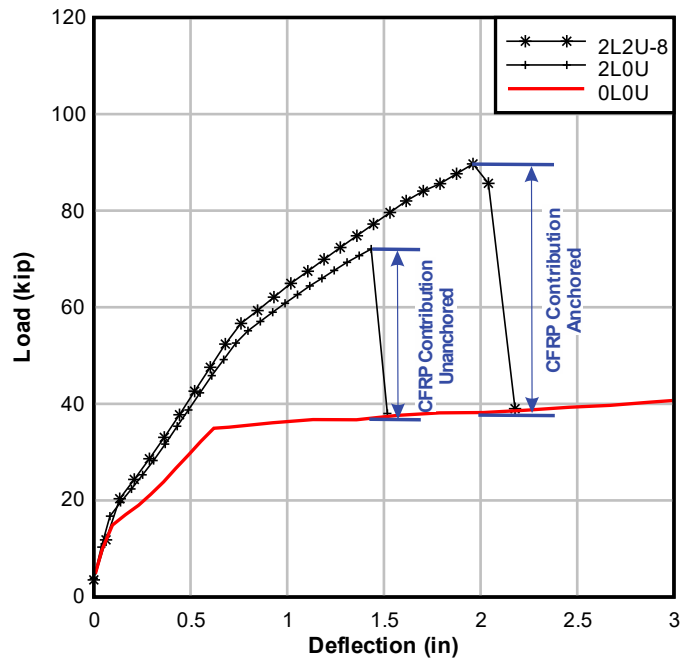
Figure 63. Comparison of strain of the steel and concrete from the Response-2000 model to the ACI 318 tension-controlled limits.

## COMPARISON TO LITERATURE

Four studies within the available literature data were used to compare the experimental results from this study (Yalim et al., 2008; Demakos et al., 2013; Rasheed et al., 2015; Hasnat et al., 2016). Each of these studies investigated the effectiveness of U-Wraps as a means of anchorage for flexural CFRP. These studies tested girders with span lengths ranging from 3½ ft to 16 ft. The literature data was limited to these studies, as each study required a reinforced concrete control girder and an unanchored strengthened control girder to compare against the experimental results from this study.

The contribution of CFRP to the flexural capacity of a girder was evaluated considering only the contribution of the longitudinal CFRP to the total moment capacity. A flexural member exhibits a reduction of stiffness once the tensile steel reinforcement reaches its yield stress. Any increase in strength that occurs after the yield of the tensile steel reinforcement is then due to the strain hardening behavior of the tensile steel reinforcement and tension stiffening of the concrete. To isolate the contribution of the longitudinal CFRP to the total moment capacity of the girder, the ultimate load of a strengthened girder was compared to the load of the unstrengthened control girder *at the same deflection of the strengthened control girder* (Figure 64). This method removes any residual strength that comes after the yield of the steel reinforcement and results in the moment contribution of exclusively the longitudinal CFRP, herein referred to as the CFRP

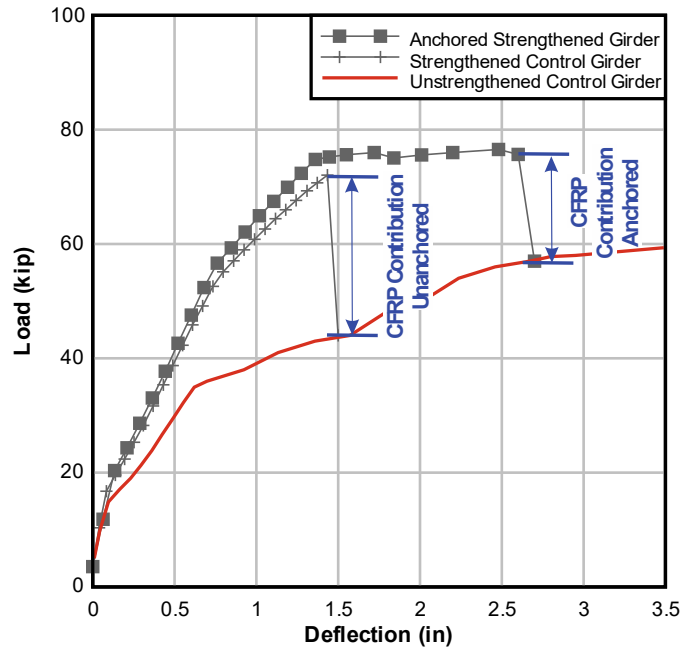
contribution. The CFRP contribution of the strengthened girders with U-Wraps was then normalized to the CFRP contribution of the unanchored control girders.



**Figure 64. Load versus midspan deflection plot used to illustrate calculation of the CFRP contribution.**

The amount of U-Wrap anchorage provided on a girder was normalized with the anchorage ratio. The anchorage ratio correlates the area of U-Wraps provided to the area of longitudinal CFRP provided on a girder. Figure 65 shows a plot of normalized CFRP contribution versus the anchorage ratio. Figure 65 includes the specimens within the 4 studies previously listed in addition to the 8 anchored girders tested in this study, which are indicated with red ellipses within the plot for a total of 28 data points. The failure modes that were observed among these specimens were IC debonding of the longitudinal CFRP; rupture of the longitudinal CFRP; failure of the U-Wrap anchor, which includes both U-Wrap rupture and U-Wrap debonding; and lastly, failure by concrete crushing. The data used in Figure 65 can be seen in





**Figure 66. Graphical representation of effect of unstrengthened control beam strain hardening behavior on the apparent CFRP contribution to the overall load capacity.**

Most of the specimens in Figure 65 show an increase in CFRP contribution due to the addition of U-Wraps to the longitudinal CFRP. Increases in CFRP contribution to the overall strength of the girders ranged between 6% and 93% (Yalim et al., 2008; Hasnat et al., 2016, respectively). While there are no clear trends within the literature data, it can be observed that IC debonding of the longitudinal CFRP is generally mitigated, and other failure modes such as complete and partial U-Wrap debonding, U-Wrap interface failure, rupture of the U-Wrap, and rupture of the longitudinal CFRP begin to control at an anchorage ratio of approximately 1.50. No further increases in strength were observed when the anchorage ratio exceeded values greater than approximately 1.50. Large anchorage ratios can be achieved by either fully wrapping a beam, providing U-Wraps in the constant moment region of the girder, or providing U-Wraps with multiple plies of CFRP, all of which are seen within the literature data or the experimental data. It was shown that fully wrapping a girder causes more of a decrease in ductility rather than an increase in strength (Foerster, 2019). Furthermore, U-Wraps placed within the constant moment region were shown to provide negligible strength gain (Hasnat et al., 2016). As previously stated, the experimental data shows that increasing the number of plies in the U-Wraps did not result in a notable increase in strength gain after U-Wrap rupture was mitigated.

The lack of uniformity among the literature data when compared to the experimental data can be attributed to multiple factors. Only Rasheed et al. (2015) completed their experimental testing at a structural scale, as the girders had a 16-ft span. The remaining studies were completed at a small scale with the spans of the girders varying from 3.5 ft to 6.5 ft. Furthermore, these studies investigated multiple variables pertaining to flexural CFRP and U-Wraps other than the amount of anchorage compared to the amount of longitudinal CFRP provided on a girder. Between the studies, the strengthened girders had U-Wraps located just at the ends of the flexural CFRP laminate, U-Wraps evenly spaced throughout the shear spans of the girder as shown in this study, and girders with their shear spans fully wrapped with a single continuous U-Wrap. As shown in Hasnat et al. (2016), placement of the U-Wraps can impact the strength gain of a flexurally strengthened girder. Future experimental testing should include evenly spaced U-Wraps within the shear spans on girders of a structural scale to confirm the findings drawn from Figure 65.

Further analysis of the literature data was conducted to investigate the increase in the load capacity due to the addition of U-Wraps to the longitudinal CFRP. The results from a total of eight studies that tested U-Wraps as flexural anchors and the experimental data were compiled (Yalim et al., 2008; Demakos et al., 2013; Rasheed et al., 2015; Hasnat et al., 2016; Breña et al., 2003; Fu, Teng, et al., 2017; Fu et al., 2018). This resulted in a total of 30 specimens that were flexurally strengthened and anchored with U-Wraps compared to the eight anchored specimens tested in this study.

The moment capacity of the flexurally strengthened girders in the literature data was calculated per ACI Committee 440 (2017). ACI Committee 440 (2017) currently limits the strength contribution of the CFRP in flexural design to the strain at which the longitudinal CFRP debonds from the concrete substrate. As observed in Figure 52 and Figure 58, the girders with U-Wrap anchors had increases in both load capacity and strain of the longitudinal CFRP when compared to their respective unanchored control girders. In herein reported experimental data, the anchored specimens exceeded the strain of their unanchored control girders between 40% and 57%. The unanchored control girders each failed by IC debonding (debonding); therefore, the anchored girders exceeded their experimental debonding strains between 40% and 57%. The debonding strain was multiplied by a factor  $\kappa_U$  to account for the increase in strain of the longitudinal CFRP, which also accounts for the increase in moment contribution of the CFRP. The experimental data showed a lower bound of increase in strain of the longitudinal CFRP of 40%. Therefore,  $\kappa_U$  was chosen to have a value of 1.40. Equation 6 shows the equation presented in ACI Committee 440 (2017) to estimate the debonding of strain of longitudinal CFRP multiplied by the factor  $\kappa_U$  to account for the increase in strain due to the addition of U-Wrap anchors (ACI Committee 440, 2017).

$$\varepsilon_{fd} = 0.083\kappa_U \sqrt{\frac{f'_c}{nE_f t_f}} \leq 0.9\varepsilon_{fu} \quad 6$$

where  $\varepsilon_{fd}$  and  $\varepsilon_{fu}$  are the debonding strain and the design rupture strain of the CFRP, respectively,  $f'_c$  is the compressive strength of the concrete,  $n$  is the number of plies of the longitudinal CFRP,  $E_f$  is the elastic modulus of the CFRP, and  $t_f$  is the nominal thickness of one ply of the CFRP. The design rupture strain is computed by multiplying the ultimate rupture strain of the CFRP by an environmental reduction factor,  $C_E$ .

The factor  $\kappa_U$  was included when calculating the CFRP contribution of the moment capacity for each of the specimens within the literature data and experimental data. (a)

(b)

Figure 67 shows the predicted moment capacity ( $M_{pred}$ ) using the factor  $\kappa_U$  applied to the debonding strain plotted against the experimental moment capacity ( $M_{exp}$ ). The values for calculated moment capacities and the experimental moment capacities can be seen in Table 11 in the appendix. It should be noted that the experimental values of the yield stress of the longitudinal steel reinforcement presented in the studies were used to calculate  $M_{pred}$ . This resulted in less conservative estimates of  $M_{pred}$ , as 60 ksi steel is typically assumed in reinforced concrete beam design.

As seen in

(a)

(b)

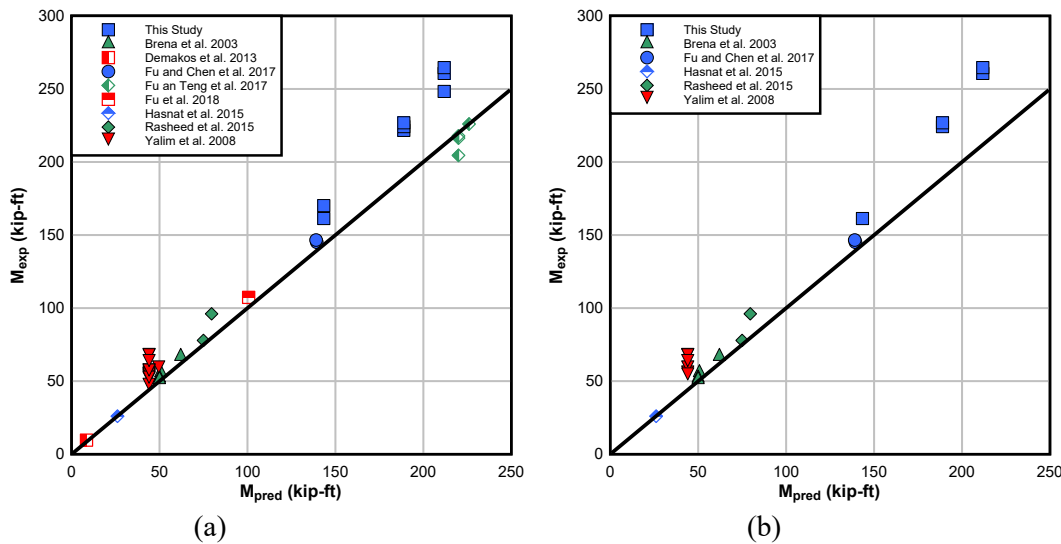
Figure 67a, the predicted moment capacities closely resembled the experimental moment capacities. The predicted moment capacity consistently resulted in conservative results when comparing it to the experimental data. In (a) (b)

Figure 67a, 5 of the 38 (or 13%) specimens included resulted in unconservative estimates of the moment capacity. The five specimens that had unconservative estimates of the moment capacity were between 1% and 8% error (average error of 2%) of the experimental moment capacity. The application of the factor  $\kappa_U$

at a value of 1.40 to the debonding strain equation resulted in conservative predictions of the increase in moment capacity due to the addition of U-Wrap anchors to the longitudinal CFRP. (a)

(b)

Figure 67b shows all the girders within the literature data and experimental data with an anchorage ratio greater than 1.50 and evenly distributed U-Wraps along the shear spans. The predicted moment capacity was unconservative in only 1 of the 19 specimens (or 5%). It should be noted that the 1 specimen that resulted in an unconservative prediction (Hasnat et al., 2016) was within 1% error of the experimental moment capacity. Although the predicted moment was unconservative, it closely reassembled the experimental moment capacity.



**Figure 67. Experimental moment capacity versus the predicted moment capacity using  $\kappa_U$  accounts for the addition of U-Wraps to the longitudinal CFRP: (a) all 38 specimens between literature data and experimental data; (b) specimens with an anchorage ratio greater than 1.50 and evenly distributed U-Wrap anchors.**

Lastly, the contribution of the CFRP to the predicted moment capacity ( $M_{nfpred}$ ) was compared to the contribution of the CFRP to the experimental moment capacity ( $M_{nfexp}$ ).  $M_{nfpred}$  was calculated by subtracting the contribution of the tensile steel reinforcement to the predicted moment capacity ( $M_{ns}$ ) from the predicted moment capacity ( $M_{pred}$ ).  $M_{nfexp}$  was calculated by subtracting the difference in load of an anchored girder at ultimate load from the load of the reinforced concrete control girder at the maximum deflection of the anchored girder. A visual representation of how  $M_{nfexp}$  was calculated is shown as the “CFRP Contribution Anchored” in Figure 64.  $M_{nfpred}$  was plotted against  $M_{nfexp}$  to evaluate if the application of the factor  $\kappa_U$  can conservatively predict the contribution of CFRP to the moment capacity when U-Wraps are applied to longitudinal CFRP ( (a)

(b)

Figure 68a).

The same 28 data points used in Figure 65 were used in (a)

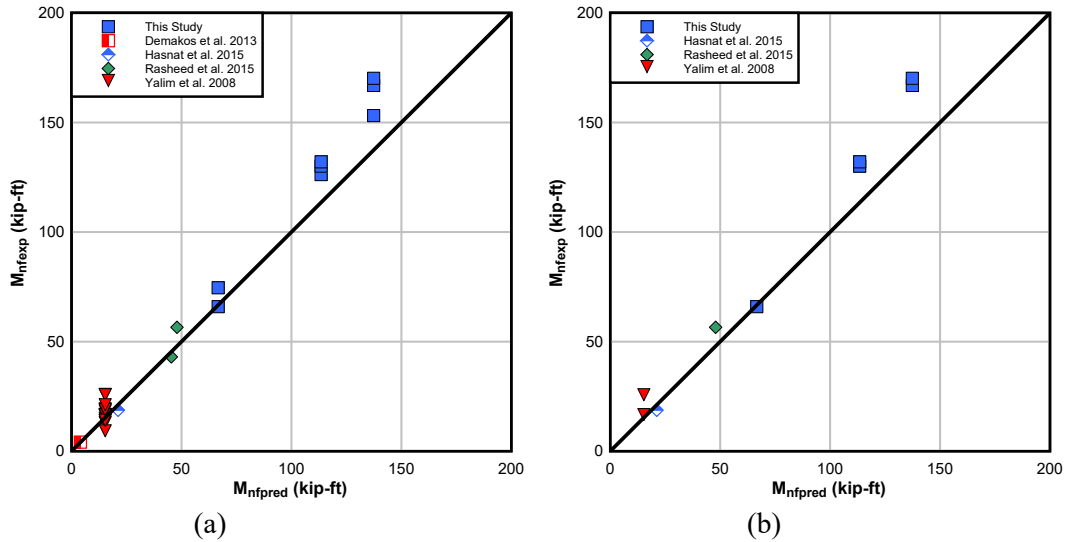
(b)

Figure 68a, since it is required to have a plain reinforced concrete control girder within the study to compute  $M_{nfexp}$ . There was a total of 7 out of the 28 (or 25%) specimens where the predicted contribution of CFRP

to the moment capacity was unconservative. The unconservative estimates can be attributed to how the  $M_{n\text{fexp}}$  was computed. The only way to isolate the experimental CFRP contribution to the moment capacity from the strain hardening behavior of the tensile steel reinforcement is through the method shown in Figure 64. There could be variations in the material properties of the concrete and steel between the reinforced concrete control girder and the anchored girder, which may have resulted in less conservative predictions of  $M_{n\text{fpred}}$ . Furthermore, five of the seven specimens that were unconservative were from the study by Yalim et al. (2008). This study investigated the effect different concrete surface profiles had on strengthened girders with U-Wrap anchorage. ACI Committee 440 (2017) recommends a concrete surface profile of at least 3 prior to the installation of CFRP. Yalim et al. (2008) included girders without any surface preparation (CSP of 1), with a concrete surface profile between CSP 2 and 3, and with a concrete surface profile between CSP 6 and 9. It should be noted that a concrete surface profile between 6 and 9 was assumed to exceed the localized out-of-plane variations limit of 1/32 in. as presented in ACI Committee 440 (2017).

(a) (b)  
 Figure 68b includes 9 of the 28 specimens in (a) (b)  
 (b)  
 Figure 68a, all of which have an anchorage ratio greater than 1.50, evenly distributed U-Wrap anchors, and meet the surface preparation guidelines presented by ACI Committee 440 (2017). A total of 2 out of the 9 specimens (or 22%) in (a) (b)  
 Figure 68b had unconservative estimates of  $M_{n\text{fpred}}$  when compared to  $M_{n\text{fexp}}$ . Girder 1L1U-8 within this study resulted in an unconservative estimate of the CFRP contribution to the moment capacity; however, it was within 1% error of  $M_{n\text{fexp}}$ . The other specimen that had an unconservative estimate of the CFRP contribution to the moment capacity was from Hasnat et al. (2016). This specimen was within 13% error of  $M_{n\text{fexp}}$ . The error can be attributed to the fact that this girder failed by anchor rupture due to the girder being heavily anchored with a single continuous U-Wrap covering each shear region of the girder.

Applying the factor  $\kappa_U$  (at a value of 1.40) to the debonding strain equation resulted in generally conservative estimates of predicted moment capacity when accounting for the addition of U-Wrap anchors to the longitudinal CFRP. However, there is a need for more experimental data to populate (a) (b)  
 Figure 67 and (a) (b)  
 Figure 68. The experimental data should be at a structural scale and using evenly distributed U-Wrap anchors to ensure that the factor  $\kappa_U$  is universally applicable.



**Figure 68. Predicted versus experimental values of the CFRP contribution to the moment capacity: (a) all 28 specimens from the literature and experimental data reviewed; (b) 9 of the 28 specimens that had an anchorage ratio of at least 1.50, had evenly distributed -Wraps, and met the surface preparation guidelines presented by ACI Committee 440 (2017).**



## CHAPTER 7

# Summary and Conclusions

### SUMMARY

The use of CFRP composites to externally strengthen bridges has become more common over recent years due to their relatively easy installation process, reduced cost compared to complete or partial component replacement, corrosion resistance, and high strength-to-weight ratio. The governing failure mode of a girder flexurally strengthened with CFRP is usually IC debonding. This failure mode greatly limits the capacity of the strengthened member as failure occurs well before the rupture strain of the flexural CFRP. The use of U-Wraps as flexural anchors has been shown to mitigate IC debonding as a failure mode and leads to a greater strain utilization of the flexural CFRP. However, there are currently no design guidelines for U-Wraps as flexural anchors, although multiple studies have investigated this topic in small-scale experiments. This experimental study investigated U-Wraps as flexural anchors for structural-scale concrete girders flexurally strengthened with CFRP.

The research program consisted of testing 12 structural-scale reinforced concrete girders strengthened with externally bonded CFRP. The study used four of the girders for both unstrengthened and strengthened control specimens and the remaining eight girders were strengthened and then anchored with U-Wraps. A 3D DIC system was used during the experimental testing to capture and analyze strains and displacements along the length of the girder. The experimental data obtained from this study were then: (i) compared to the available literature data; (ii) compared to analytical models created in Response-2000; and (iii) evaluated to make design recommendations for U-Wraps as flexural anchors.

The addition of unanchored longitudinal CFRP to the reinforced concrete girder resulted in increases of load capacity ranging from 28% to 98% compared to reinforced concrete control girder. However, the increase in load capacity came at an expense of ductility, which was reduced as much as 80% compared to the girder strengthened with one ply of longitudinal CFRP. Each of the unanchored control girders failed by IC debonding. U-Wrap anchors allowed each of the remaining girders to exceed the recorded debonding strains. Increases in strain ranging from 40% to 57% were observed when comparing the anchored girders to their respective unanchored control girders.

The anchored specimens strengthened with 1 ply of longitudinal CFRP each failed by rupture of the longitudinal CFRP. Increases in load capacity of 14% and 20% were recorded for the girders strengthened with 1 ply of longitudinal CFRP and U-Wraps at 8 in. on-center and 16 in. on-center, respectively. The remaining anchored girders were strengthened with 2 or 3 plies of longitudinal CFRP. Each of these girders reached its ultimate load capacity when failure of the U-Wrap anchors occurred. Anchor failure includes partial or completed debonding of the U-Wraps and rupture of the U-Wraps. Increases in load capacity ranged from 14% to 25%, and increases in strain of the longitudinal CFRP ranged from 40% to 49% compared to the corresponding unanchored control girder.

## CONCLUSIONS

The following are the main conclusions drawn from this experimental program:

- Unanchored longitudinal CFRP increased the load capacity of the reinforced concrete girder between 28% and 98%.
- The addition of longitudinal CFRP decreased ductility as much as 80%.
- The addition of U-Wraps resulted in an increase of the maximum strain of the longitudinal CFRP between 40% and 57% compared to the respective unanchored control girders.
- U-Wrap anchorage allowed the longitudinal CFRP to exceed the calculated ACI 440 debonding strain ranging from 65% to 123%.
- Addition of U-Wraps increased the ultimate load capacity of girders between 14% and 25% when compared to their respective unanchored control girders.
- U-Wraps shifted the failure mode of strengthened girders from IC debonding to rupture of the longitudinal CFRP, complete or partial debonding of the U-Wraps, rupture of the U-Wraps, or failure of the adhesive bond between the longitudinal CFRP and the U-Wraps.
- Analysis of the literature data indicates that IC debonding may be mitigated when the anchorage ratio exceeds 1.50.
- The literature data showed little apparent increase in load capacity when the anchorage ratio exceeded 1.50. The observed increases in moment capacity varied between 3% and 63% among the specimens with anchorage ratios of 1.50 to 5.2 without any correlation between the anchorage ratio to the increase in the moment capacity.

## CHAPTER 8

# Recommendations for Future Work

The completed experimental program showed the effectiveness of U-Wraps as flexural anchors. However, further research should be conducted to confirm that the findings and design recommendations presented in this study are applicable beyond the bounds of this work and other studies from the literature. The following outlines recommendations for future work based on the experience of this research study:

- The lower bounds of the anchorage ratio (i.e.  $< 1.50$ ) should be investigated. Although the literature data showed that IC debonding was noticeably mitigated at an anchorage ratio of 1.50, the literature data explored multiple variables related to U-Wraps other than the ones investigated in this study. Furthermore, the lower bounds of the anchorage ratio should be explored with structural-scale specimens and U-Wraps evenly spaced within the shear spans.
- Since it is recommended to explore the lower bounds of the anchorage ratio, a larger spacing of the U-Wraps could naturally be investigated. The design recommendations listed in this chapter mention spacing the U-Wraps less than or equal to the depth of the reinforcing steel,  $d$ , while still adhering to the requirements for U-Wraps as shear reinforcement presented in ACI Committee 440 (2017). Most of the U-Wraps in this study were spaced at 8 in. ( $d/2$ ), which adhered to the maximum spacing of U-Wraps as shear reinforcement. The 1L2U-16 girder was the only girder with U-Wraps spaced at 16 in. ( $d$ ) on-center within the experimental study. 1L2U-16 provided both a greater load capacity and ductility compared to 1L1U-8, which had an identical total cross-sectional area of U-Wraps as 1L2U-16. It can be theorized that the larger spacing of U-Wraps allowed for a greater load capacity and ductility of the strengthened girder. However, further analysis and experimental data are needed to confirm this.
- The concrete girder used in this study was lightly reinforced with a reinforcement ratio of 0.0045. The girder was purposely lightly reinforced to maximize the strength gain due to the addition of flexural CFRP. A girder of this nature would typically not be designed in practice due to deflection limits and cost-effective design. Future experimental studies would benefit from using a more heavily reinforced concrete section that is tension-controlled. Furthermore, future experimental studies would also benefit from testing more common beam and girder geometries such as T-beams or AASHTO girders.
- The girders in this study were heavily reinforced in shear to ensure that a shear failure would not occur when accounting for the increase in applied load due to the addition of longitudinal CFRP. U-Wraps were used in this study as flexural anchors; however, U-Wraps are more commonly used in shear strengthening of reinforced concrete girders. Future studies would benefit from using shear deficient girders to investigate whether U-Wraps can simultaneously be used as flexural anchorage and shear reinforcement.

# References


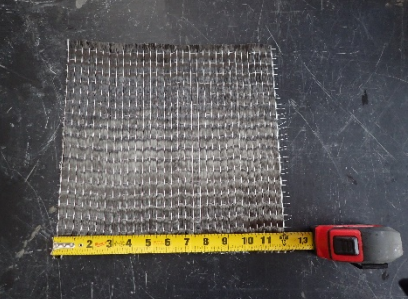
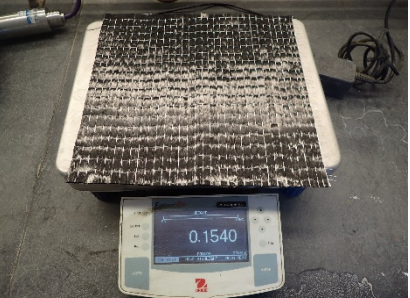

- ACI Committee 318. Building Code Requirements for Structural Concrete: (ACI 318- 19) ; and Commentary (ACI 318-19). Farmington Hills, MI: American Concrete Institute, 2019.
- ACI Committee 440. Guide for Design and Construction of Externally Bonded FRP Systems for Strengthening of Concrete Structures: (ACI 440.2R-17) ; and Commentary (ACI 440.2R-17). Farmington Hills, MI :American Concrete Institute, 2017.
- Al-Amery, R., & Al-Mahaidi, R. (2006). Coupled flexural-shear retrofitting of RC beams using CFRP straps. *Composite Structures*, 75(1–4), 457–464.
- Bentz (2000) PhD dissertation. Bentz, E. C. (2000). *Sectional analysis of reinforced concrete members* (p. 310). Toronto: University of Toronto.
- Breña, S. F., Bramblett, R. M., Wood, S. L., & Kreger, M. E. (2003). Increasing Flexural Capacity of Reinforced Concrete Beams Using Carbon Fiber-Reinforced Polymer Composites. Paper by Sergio F. Breña, Regan M. Bramblett, Sharon L. Wood, and Michael E. Kreger. *ACI Structural Journal*, 100(6), 827–830.
- del Rey Castillo, E., Kanitkar, R., Smith, S. T., Griffith, M. C., & Ingham, J. M. (2019). Design approach for FRP spike anchors in FRP-strengthened RC structures. *Composite Structures*, 214(January), 23–33.
- Concrete Protection & Repair Services (2019). CPR Services: Concrete Protection & Repair Services, <<http://cpaustralia.com.au/services/carbon-fibre-reinforcement/>> (accessed 15 October 2019).
- Demakos, C. B., Repapis, C. C., & Drivas, D. (2013). Investigation of Structural Response of Reinforced Concrete Beams Strengthened with Anchored FRPs. *The Open Construction and Building Technology Journal*, 7(1), 146–157.
- Florida International University (2019). Accelerated Bridge Construction, <[https://abc-utc.fiu.edu/mc-events/michigan-dots-use-of-externally-bonded-frp-systems-for-bridge-element-strengthening/?mc\\_id=493](https://abc-utc.fiu.edu/mc-events/michigan-dots-use-of-externally-bonded-frp-systems-for-bridge-element-strengthening/?mc_id=493)> (accessed 31 October 2019).
- Foerster, A. S. (2019). *Strengthening reinforced concrete bridge T-beams with CFRP sheets plus bi-directional CFRP U-Wraps*. Kansas State University.
- Fu, B., Chen, G. M., & Teng, J. G. (2017). Mitigation of intermediate crack debonding in FRP-plated RC beams using FRP U-jackets. *Composite Structures*, 176, 883–897.
- Fu, B., Tang, X. T., Li, L. J., Liu, F., & Lin, G. (2018). Inclined FRP U-jackets for enhancing structural performance of FRP-plated RC beams suffering from IC debonding. *Composite Structures*, 200(June 2017), 36–46.
- Fu, B., Teng, J. G., Chen, J. F., Chen, G. M., & Guo, Y. C. (2017). Concrete Cover Separation in FRP-Plated RC Beams: Mitigation Using FRP U-Jackets. *Journal of Composites for Construction*, 21(2), 04016077.
- Haddad, R. H., & Marji, C. S. (2019). Composite Strips with U-Shaped CFRP Wrap Anchor Systems for Strengthening Reinforced Concrete Beams. *International Journal of Civil Engineering*, 17(11), 1799–1811.

- Hasnat, A., Islam, M. M., & Amin, A. F. M. S. (2016). Enhancing the Debonding Strain Limit for CFRP-Strengthened RC Beams Using U-Clamps: Identification of Design Parameters. *Journal of Composites for Construction*, 20(1), 04015039.
- International Concrete Repair Institute (2013). Selecting and Specifying Concrete Surface Preparation for Sealers, Coatings, Polymer Overlays, and Concrete Repair. Guideline No. 310.2R-2013. St. Paul, MN: International Concrete Repair Institute, 2013
- Jirsa, J. O., Shekarchi, W. A., Pudleiner, D. K., & Wang, H. (2017). *Use of Carbon Fiber Reinforced Polymer ( CFRP ) with CFRP Anchors for Shear-Strengthening and Design Recommendations / Quality Control Procedures for CFRP Anchors*. 0, 1–278.
- Kalfat, R., Gadd, J., Al-Mahaidi, R., & Smith, S. T. (2018). An efficiency framework for anchorage devices used to enhance the performance of FRP strengthened RC members. *Construction and Building Materials*, 191, 354–375.
- Lee, J., & Lopez, M. M. (2016). Characterization of FRP Uwrap Anchors for Externally Bonded FRP-Reinforced Concrete Elements: An Experimental Study. *Journal of Composites for Construction*, 20(4), 04016012.
- Lee, J., & Lopez, M. M. (2019). Frictional bond-slip model for the concrete-FRP interface under the FRP U-wrap region. *Construction and Building Materials*, 194, 226–237.
- Liu, I. S. T., Oehlers, D. J., & Seracino, R. (2007). Study of Intermediate Crack Debonding in Adhesively Plated Beams. *Journal of Composites for Construction*, 11(2), 175–183.
- Niemitz, C. W., James, R., & Breña, S. F. (2010). Experimental Behavior of Carbon Fiber-Reinforced Polymer (CFRP) Sheets Attached to Concrete Surfaces Using CFRP Anchors. *Journal of Composites for Construction*, 14(2), 185–194.
- Ozbakkaloglu, T., Fang, C., & Gholampour, A. (2017). Influence of FRP anchor configuration on the behavior of FRP plates externally bonded on concrete members. *Engineering Structures*, 133, 133–150.
- Pan, J., Leung, C. K. Y., & Luo, M. (2010). Effect of multiple secondary cracks on FRP debonding from the substrate of reinforced concrete beams. *Construction and Building Materials*, 24(12), 2507–2516.
- Pham, H. B., & Al-Mahaidi, R. (2006). Prediction Models for Debonding Failure Loads of Carbon Fiber Reinforced Polymer Retrofitted Reinforced Concrete Beams. *Journal of Composites for Construction*, 10(1), 48–59.
- Raheem, M. M., & Rasheed, H. A. (2021). Development of an objective model to predict shear capacity of FRP U-wrap anchors. *Composite Structures*, 265(February), 113762.
- Rasheed, H. A., Decker, B. R., Esmaily, A., Peterman, R. J., & Melhem, H. G. (2015). The influence of CFRP anchorage on achieving sectional flexural capacity of strengthened concrete beams. *Fibers*, 3(4), 539–559.
- Sagawa, Y., Matsushita, H., and Tsuruta, H. "Anchoring Method of Carbon Fiber Sheet for Strengthening of Reinforced Concrete Beams." *Proc., Fifth International Conference on Fibre-Reinforced Plastics for Reinforced Concrete Structures*, Thomas Telford.
- Smith, S. T., Hu, S., Kim, S. J., & Seracino, R. (2011). FRP-strengthened RC slabs anchored with FRP anchors. *Engineering Structures*, 33(4), 1075–1087.
- Smith, S. T., Zhang, H., & Wang, Z. (2013). Influence of FRP anchors on the strength and ductility of FRP-strengthened RC slabs. *Construction and Building Materials*, 49, 998–1012.
- The Constructor (2020). Strengthening of RCC Beams in Shear using Externally Bonded FRP plates or Strips, <<https://theconstructor.org/structural-engg/rcc-beams-strengthening-shear-frp-plate/15148/>> (accessed 31 January 2020).


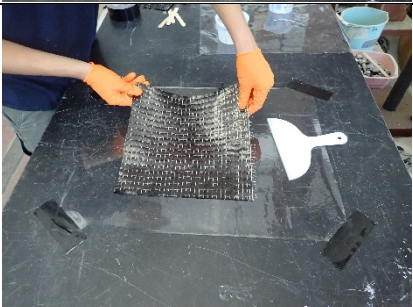


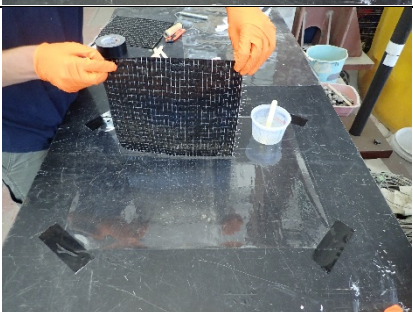
- Wang, Y. C. (2000). *Retrofit of Reinforced Concrete Members Using Advanced Composite Materials* (Issue February).
- Yalim, B., Kalayci, A. S., & Mirmiran, A. (2008). Performance of FRP-strengthened RC beams with surface out-of-flatness. *Advances in Structural Engineering*, 12(2), 241–255.
- Zaki, M. A., & Rasheed, H. A. (2019). Impact of efficiency and practicality of CFRP anchor installation techniques on the performance of RC beams strengthened with CFRP sheets. *Canadian Journal of Civil Engineering*, 46(9), 796–809.
- Zhang, H. W., & Smith, S. T. (2012). Influence of FRP anchor fan configuration and dowel angle on anchoring FRP plates. *Composites Part B: Engineering*, 43(8), 3516–3527.
- Zhang, H. W., & Smith, S. T. (2012). FRP-to-concrete joint assemblages anchored with multiple FRP anchors. *Composite Structures*, 94(2), 403–414.
- Zhang, H. W., Smith, S. T., & Kim, S. J. (2012). Optimization of carbon and glass FRP anchor design. *Construction and Building Materials*, 32, 1–12.
- Zhang, H., & Smith, S. T. (2017). Influence of plate length and anchor position on FRP-to-concrete joints anchored with FRP anchors. *Composite Structures*, 159, 615–624.

# Appendix

**Table 9. Descriptive process on the creation of witness panels.**



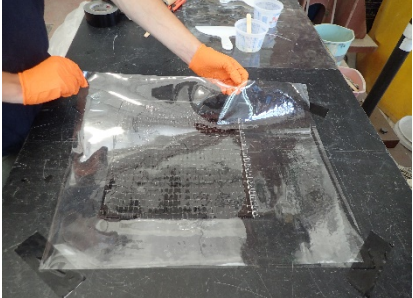
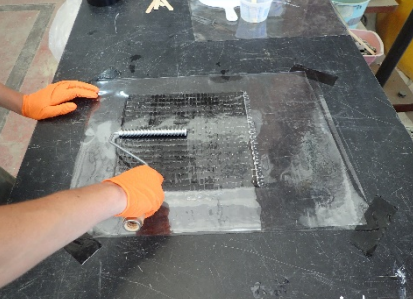
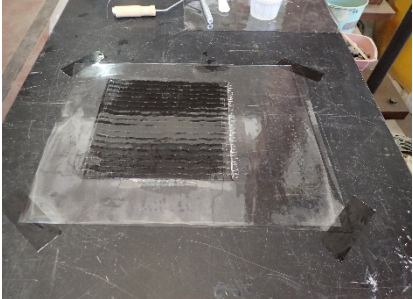
Step	Description	Visual
1) Cut 2 sheets of 16-mil plastic sheeting	a) Secured 1 of the 2 sheets of the 16-mil plastic sheeting onto the work surface. Kept the second sheet of 16-mil plastic for step 12.	
2) Cut the CFRP sheet(s)	b) Cut one (1) 12 in. by 12 in. sheet of CFRP for each layer of longitudinal CFRP installed on the girder.	
3) Weigh sheet(s) of CFRP	c) Recorded weight of CFRP sheet(s)	
4) Weigh epoxy	d) Measured out the same weight of epoxy as recorded in step 2	

**Table 9 (continued)**

Step	Description	Visual
5) Apply thin layer of epoxy onto the 16-mil plastic	e) Added small quantity of epoxy onto the plastic sheeting. Distributed the epoxy over the plastic with a putty knife.	
6) Place CFRP sheet onto plastic	f) Placed CFRP onto plastic sheeting and gently pressed into epoxy using a plastic putty knife.	
7) Add epoxy onto the CFRP sheet	g) Added approximately half of the remaining epoxy onto the CFRP sheet.	
8) Distribute epoxy onto CFRP	h) Evenly distributed epoxy over the CFRP sheet using a plastic putty knife.	
9) Flip CFRP sheet	i) Flipped CFRP sheet to saturate the other side with epoxy.	



**Table 9 (continued)**

Step	Description	Visual
10) Add epoxy to the CFRP sheet	j) Added the remaining epoxy onto the CFRP sheet	
11) Distribute epoxy onto CFRP	k) Evenly distributed epoxy over the CFRP sheet using a plastic putty knife. Repeated steps 5-11 for any additional sheets of CFRP.	
12) Place second 16-mil plastic sheeting over CFRP	l) Covered the CFRP sheet with the 16-mil plastic sheet.	
13) Use roller to distribute epoxy	m) Used a roller over the plastic sheeting to further distribute the epoxy.	
14) Allow the witness panel cure	n) Allowed the witness panel to cure for a minimum of 48 hours.	



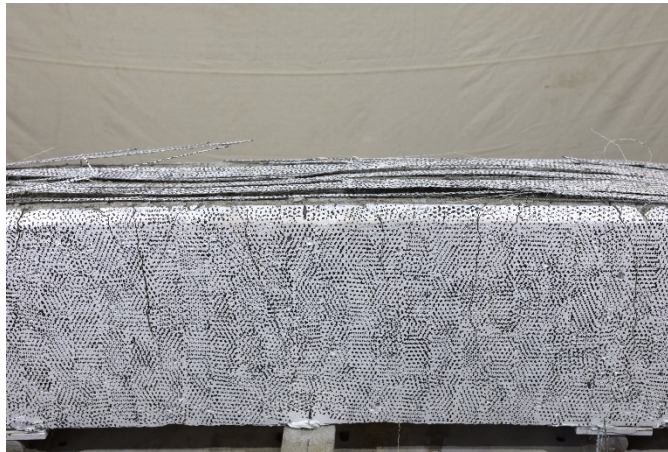
**Figure 69. Concrete crushing failure of 0L0U**



**Figure 70. IC debonding failure of 1L0U**



***Figure 71. Rupture of the longitudinal CFRP within the constant moment region of 1L1U-8.***



***Figure 72. Rupture of the longitudinal CFRP within the constant moment region of 1L2U-16.***



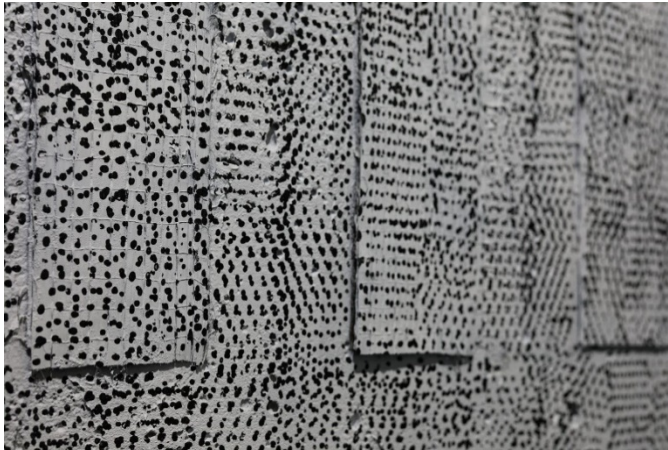
**Figure 73. IC debonding failure of 2L0U. Girder was taken to concrete crushing post-debonding failure to investigate its residual strength.**



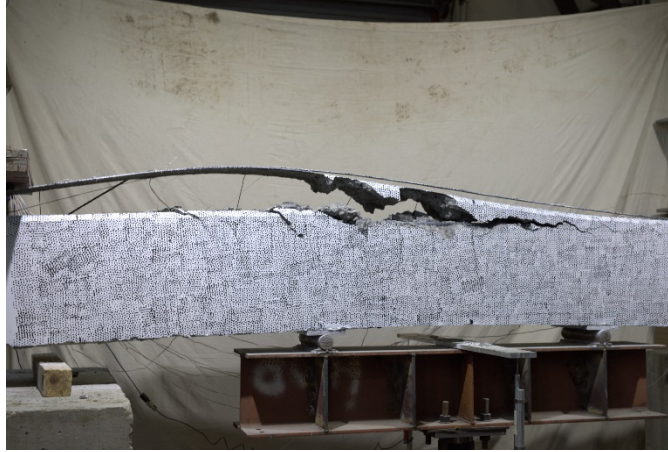
**Figure 74. U-Wrap rupture failure of 2L1U-8.**



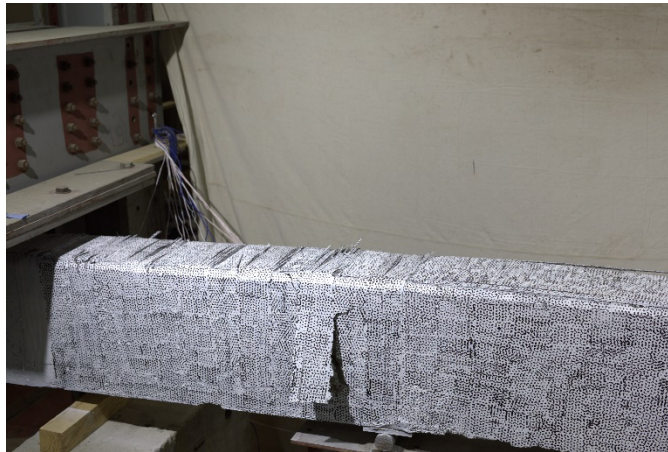
**Figure 75. Complete U-Wrap debonding failure of 2L2U-8.**



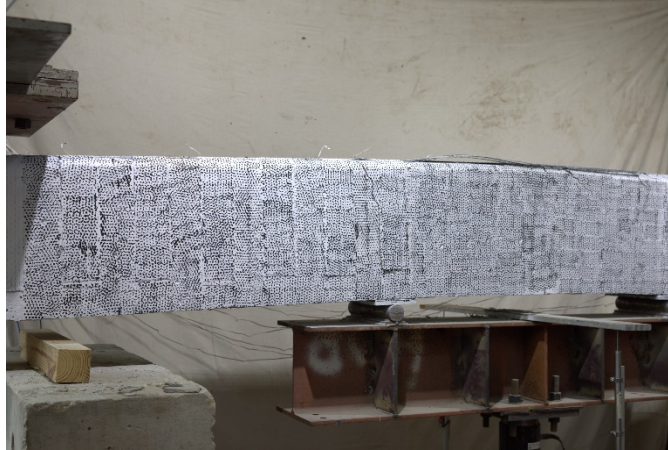
**Figure 76. Partial U-Wrap debonding failure of 2L3U-8.**



**Figure 77. IC debonding failure of 3L0U.**



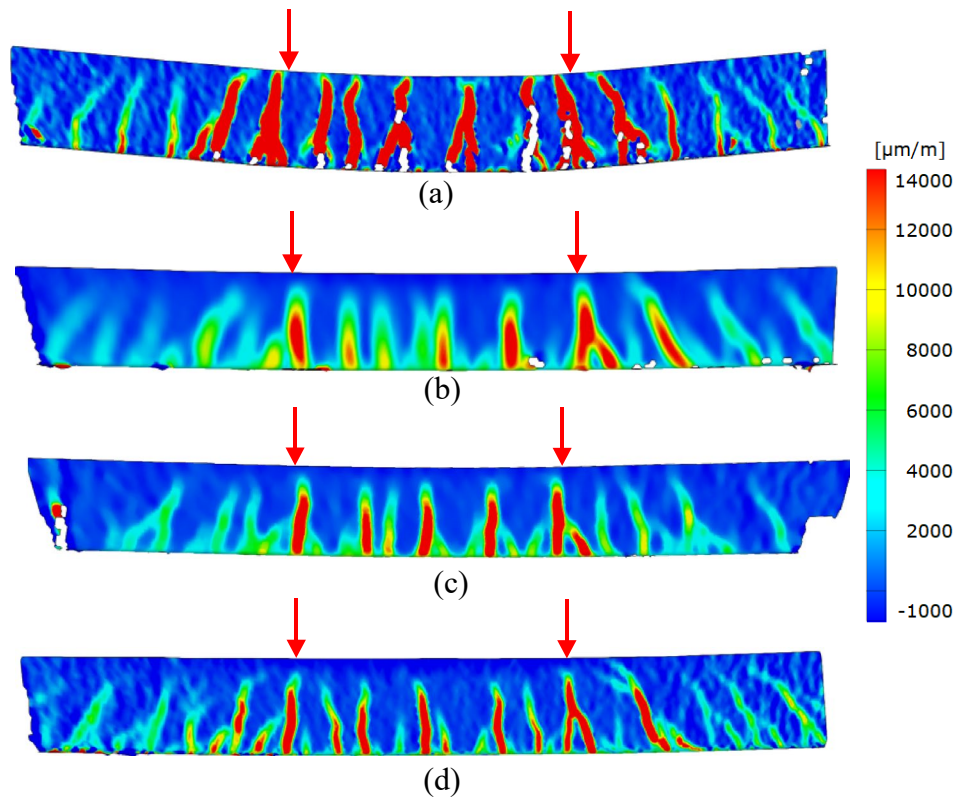
**Figure 78. U-Wrap rupture failure of 3L1U-8.**



**Figure 79. Complete U-Wrap debonding failure of 3L2U-8.**

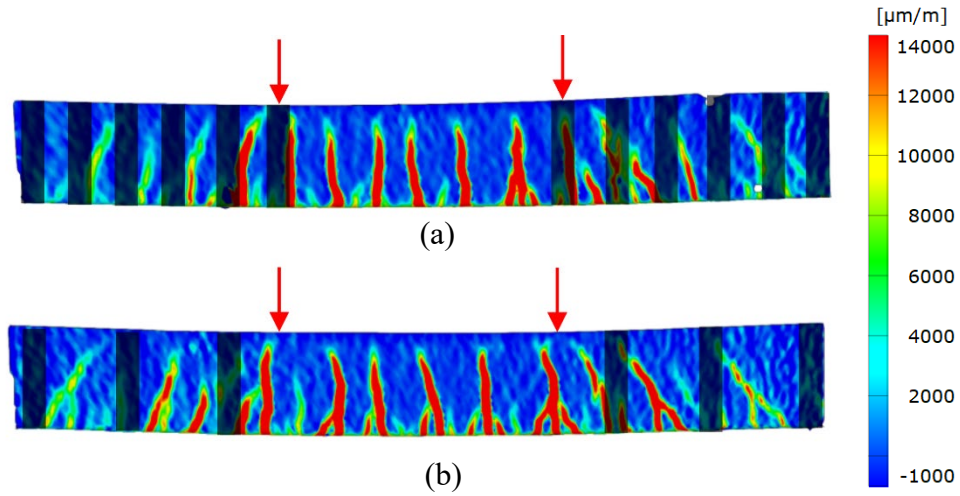


**Figure 80. Concrete crushing failure of 3L3U-8. Secondary failure mode of complete U-Wrap debonding was observed.**

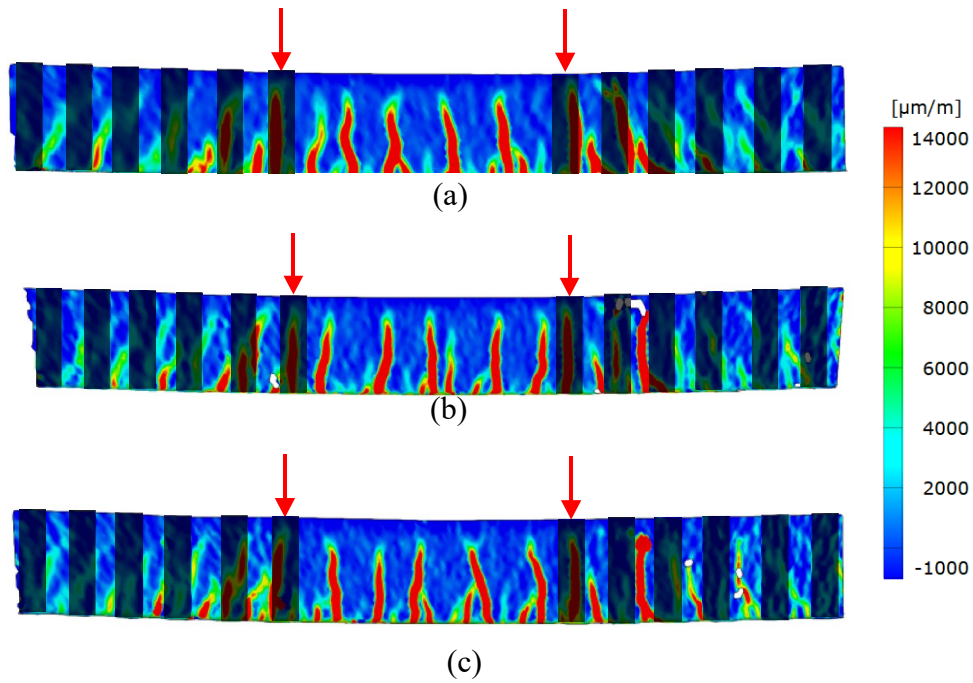


**Figure 81. Crack patterns of the control girders (arrows represent the approximate locations of the loading points on the girder): (a) Girder 0L0U; (b) Girder 1L0U; (c) Girder 2L0U; (d) Girder 3L0U.**

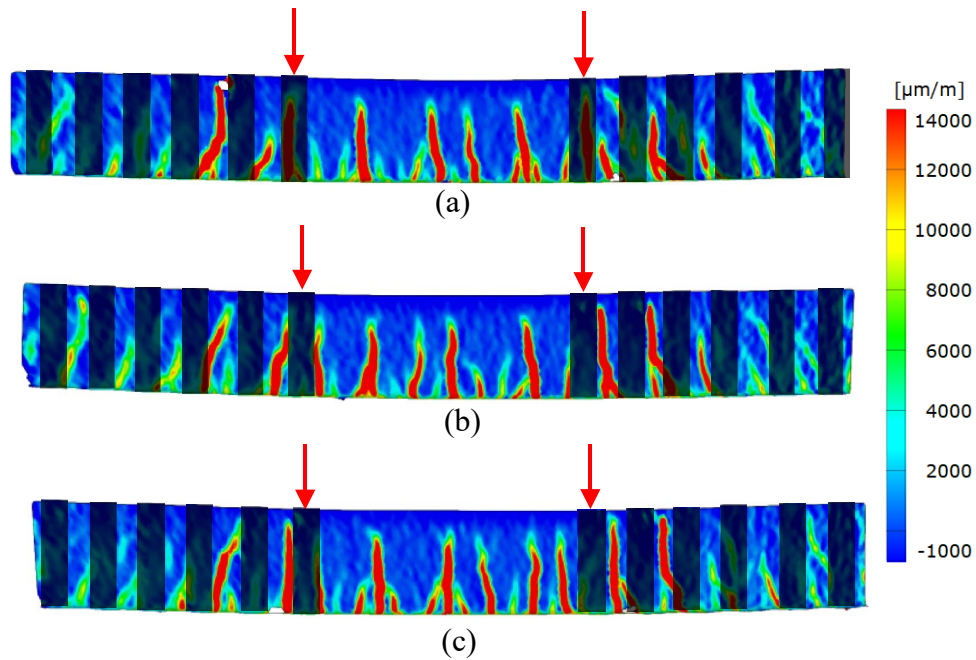




**Figure 82. Crack patterns of the girders strengthened with 1 ply of longitudinal CFRP (arrows represent the approximate locations of the loading points on the girder and the shaded bars represent the approximate locations of the U-Wraps): (a) Girder 1L1U-8; (b) Girder 1L2U-16.**



**Figure 83. Crack patterns of the girders strengthened with 2 plies of longitudinal CFRP (arrows represent the approximate locations of the loading points on the girder and the shaded bars represent the approximate locations of the U-Wraps): (a) Girder 2L1U-8; (b) Girder 2L2U-8; (c) Girder 2L3U-8.**



**Figure 84. Crack patterns of the girders strengthened with 3 plies of longitudinal CFRP (arrows represent the approximate locations of the loading points on the girder and the shaded bars represent the approximate locations of the U-Wraps): (a) Girder 3L1U-8; (b) Girder 3L2U-8; (c) Girder 3L3U-8.**

**Table 10. Experimental data and literature data used in Figure 65.**

Study	Specimen	Normalized CFRP Contribution	$A_{prov}$ (in <sup>2</sup> )	$A_{fanchor}$ (in <sup>2</sup> )	$A_{prov} / A_{fanchor}$	Failure Mode
This Study	1L1U-8	1.37	2.56	1.23	2.08	RP
	1L2U-16	1.56	2.56	1.77	1.45	RP
	2L1U-8	1.41	2.56	1.74	1.47	UR
	2L2U-8	1.45	5.12	2.51	2.04	UCD
	2L3U-8	1.48	7.68	3.13	2.45	UPD & UIF
	3L1U-8	1.23	2.56	2.13	1.20	UR
	3L2U-8	1.34	5.12	3.07	1.67	UCD
	3L3U-8	1.36	7.68	3.83	2.00	CC
Demakos et al. 2013	B1/CFRP/CMAS	1.38	0.15	0.20	0.79	IC
Hasnat et al. 2016	S(AT3c)WC	1.93	0.55	0.26	2.08	UR
Rasheed et al. 2015	T3	1.54	0.65	0.40	1.63	RP
	R3	1.18	0.36	0.27	1.34	CC & RP
Yalim et al. 2008	CSP1 4 U-Wraps	0.97	0.65	0.52	1.23	IC
	CSP1 4 U-Wraps	0.90	0.65	0.52	1.22	IC
	CSP1 4 U-Wraps	1.08	0.65	0.52	1.23	IC
	CSP1 7 U-Wraps	0.83	0.97	0.52	1.84	IC
	CSP1 11 U-Wraps	1.26	1.61	0.52	3.07	RP
	CSP1 Full U-Wraps	1.72	2.71	0.52	5.17	RP
	CSP2-3 4 U-Wraps	1.04	0.65	0.52	1.23	IC
	CSP2-3 4 U-Wraps	1.10	0.65	0.52	1.23	IC
	CSP2-3 4 U-Wraps	0.58	0.65	0.52	1.23	IC
	CSP2-3 11 U-Wraps	1.09	1.61	0.52	3.07	RP
	CSP2-3 Full U-Wraps	1.71	2.71	0.52	5.17	RP
	CSP6-9 4 U-Wraps	1.20	0.65	0.52	1.23	IC
	CSP6-9 4 U-Wraps	0.91	0.65	0.52	1.23	IC
	CSP6-9 4 U-Wraps	1.25	0.65	0.52	1.23	IC
	CSP6-9 11 U-Wraps	1.39	1.61	0.52	3.07	RP

RP : Rupture of the longitudinal CFRP  
 UR : Rupture of the U-Wrap anchor  
 UPD : Partial debonding of the U-Wrap anchor  
 UCD : Complete debonding of the U-Wrap anchor  
 UIF : U-Wrap interface failure  
 IC : Intermediate crack debonding  
 CC : Concrete crushing

**Table 11. Experimental data and literature data used in**  
**(b)**

**(a)**

**Figure 67.**

Study	Specimen	$M_n$	$M_{pred}$	$M_{exp}$	$M_{pred} / M_{exp}$	Failure Mode
		(kip-ft)	(kip-ft)	(kip-ft)		
This Study	1L1U-8	134.94	143.39	161.30	1.12	RP
	1L2U-16	134.94	143.39	170.15	1.18	RP
	2L1U-8	156.47	188.89	221.65	1.17	UR
	2L2U-8	156.47	188.89	224.19	1.18	UCD
	2L3U-8	156.47	188.89	226.85	1.20	UPD & UIF
	3L1U-8	172.56	211.82	248.28	1.17	UR
	3L2U-8	172.56	211.82	260.60	1.23	UCD
	3L3U-8	172.56	211.82	264.59	1.25	CC
Breña et al., 2003	B2	47.12	50.70	55.82	1.10	RP
	B4	46.54	49.97	52.15	1.04	RP
	B5	46.54	49.97	51.10	1.02	RP
	C3	56.95	62.08	67.00	1.08	RP
Demakos et al., 2013	B1/CFRP/CMAS	6.22	6.92	9.62	1.39	IC
Fu, Chen, et al., 2017	V1L1W120	188.21	226.02	225.98	0.99	IC
	V1L1W60	183.85	219.99	204.51	0.92	IC
	V1L1W90	183.85	219.99	216.39	0.98	IC
	V2L1W60	183.85	219.99	217.87	0.99	IC
Fu, Teng, et al., 2017	B2S1	117.27	139.40	145.06	1.04	IC
	B3S1	116.87	139.00	146.60	1.05	RP
Fu et al., 2018	V90W150H350	83.63	100.68	107.33	1.07	IC
Hasnat et al., 2016	S(AT3c)C	20.06	26.10	25.94	0.99	UR
Rasheed et al., 2015	T3	52.09	59.47	96.08	1.61	RP
	R3	48.64	55.42	77.88	1.40	CC & RP
Yalim et al., 2008	CSP1 4 U-Wraps	43.60	44.05	52.16	1.18	IC
	CSP1 4 U-Wraps	43.60	44.05	50.88	1.15	IC
	CSP1 4 U-Wraps	43.60	44.05	52.49	1.19	IC
	CSP1 7 U-Wraps	43.60	44.05	54.94	1.24	IC
	CSP1 11 U-Wraps	43.60	44.05	58.37	1.32	RP
	CSP1 Full U-Wrap	43.60	44.05	66.96	1.52	RP
	CSP2-3 4 U-Wraps	43.60	44.05	53.48	1.2	IC
	CSP2-3 4 U-Wraps	43.60	44.05	53.95	1.22	IC
	CSP2-3 4 U-Wraps	43.60	44.05	46.50	1.05	IC
	CSP2-3 11 U-Wraps	43.60	44.05	53.59	1.22	RP
	CSP2-3 Full U-Wrap	43.60	44.05	66.67	1.51	RP
	CSP6-9 4 U-Wraps	43.60	44.05	56.40	1.28	IC
	CSP6-9 4 U-Wraps	43.60	44.05	51.36	1.16	IC
	CSP6-9 4 U-Wraps	43.60	44.05	56.26	1.27	IC
CSP6-9 11 U-Wraps	43.60	44.05	62.76	1.42	RP	

RP : Rupture of the longitudinal CFRP

UR : Rupture of the U-Wrap anchor

UPD : Partial debonding of the U-Wrap anchor

UCD : Complete debonding of the U-Wrap anchor

UIF : U-Wrap interface failure

IC : Intermediate crack debonding

CC : Concrete crushing

$M_n$  : Nominal moment capacity per ACI 440.2R-17

$M_{pred}$  : Predicted moment capacity by applying a factor of 1.4 to the ACI 440.2R-17 debonding strain equation

$M_{exp}$  : Experimental moment capacit